Deep-Sea Research I 86 (2014) 1–20

Contents lists available at ScienceDirect

Deep-Sea Research I

journal homepage: www.elsevier.com/locate/dsri

Antipodal acoustic thermometry: 1960, 2004

Brian D. Dushaw [a,*], Dimitris Menemenlis [b]

[a] Applied Physics Laboratory, University of Washington, 1013 N.E. 40th Street, Seattle, WA 98105-6698, USA
[b] Jet Propulsion Laboratory, California Institute of Technology, 4800 Oak Grove Drive, Pasadena, CA 91109, USA

ARTICLE INFO

Article history:
Received 29 May 2013
Received in revised form
11 November 2013
Accepted 21 December 2013
Available online 9 January 2014

Keywords:
Antipodal acoustics
Ocean modeling
Acoustic tomography
Climate change

ABSTRACT

On 21 March 1960, sounds from three 300-lb depth charges deployed at 5.5-min intervals off Perth, Australia were recorded by the SOFAR station at Bermuda. The recorded travel time of these signals, about 13,375 s, is a historical measure of the ocean temperature averaged across several ocean basins. The 1960 travel time measurement has about 3-s precision. High-resolution global ocean state estimates for 2004 from the "Estimating the Circulation and Climate of the Ocean, Phase II" (ECCO2) project were combined with ray tracing to determine the paths followed by the acoustic signals. The acoustic paths are refracted geodesics that are slightly deflected by either small-scale topographic features in the Southern Ocean or the coast of Brazil. The refractive influences of intense, small-scale oceanographic features, such as Agulhas Rings or eddies in the Antarctic Circumpolar Current, greatly reduce the necessary topographic deflection and cause the acoustic paths to meander in time. The ECCO2 ocean state estimates, which are constrained by model dynamics and available data, were used to compute present-day travel times. Measured and computed arrival coda were in good agreement. Based on recent estimates of warming of the upper ocean, the travel-time change over the past half-century was nominally expected to be about −9 s, but little difference between measured (1960) and computed (2004) travel times was found. Taking into account uncertainties in the 1960 measurements, the 2004 ocean state estimates, and other approximations, the ocean temperature averaged along the sound channel axis over the antipodal paths has warmed at a rate less than about 4.6 m °C yr^{-1} (95% confidence). At this time, the estimated uncertainties are comparable in size to the expected warming signal, however.

1. Introduction

In 1960, an acoustics experiment conducted by scientists of the Lamont Geological Observatory of Columbia University tested the ability of acoustic signals to travel through the oceans over antipodal distances (Shockley et al., 1982; Munk et al., 1988; Heaney et al., 1991; Jensen et al., 1994; Munk et al., 1995; Dushaw, 2008). In close coordination with the Lamont scientists, a sequence of three explosive charges was deployed at 5.5-min intervals as sound sources by *HMAS Diamantina* off Perth, Australia. The signals of those charges were recorded by Lamont's Bermuda SOFAR station some 3 h 43 m later (Fig. 1). This paper has two basic goals. The first is to combine acoustic propagation techniques with recent estimates for the ocean state from a high-resolution general circulation model to better understand the signals recorded at Bermuda and their paths through the ocean. The second is to compare the travel times measured in 1960 to travel times computed in the ocean state estimates. The present-day travel time is nominally expected to be about 9 s less than the 1960 travel time, based on recent estimates of ocean warming (Levitus et al., 2000, 2005; Gille, 2008; Lyman et al., 2010). The difference between historical and present-day travel times is a measure of the change in ocean temperature over the past half century (Munk and Forbes, 1989).

The 1960 experiment represents a unique measurement of the ocean's climate state a half century ago. The measurement is a natural integration of ocean temperature over an antipodal distance. This fundamental property was the motivation for the 1991 Heard Island Feasibility Test (HIFT), a 9-day experiment which tested the ability of controlled acoustic sources to transmit sound over antipodal distances for the purposes of acoustic thermometry (Munk et al., 1994). The 1960 acoustic propagation was across a large area of the Southern Ocean, where historical in situ sampling is poor. The measurement requires a careful interpretation, however, since the acoustic pulses traveled along depths near the sound channel axis (Dushaw, 2008). Except for the region where the acoustic path crosses

* Corresponding author.
E-mail address: dushaw@apl.washington.edu (B.D. Dushaw).

0967-0637
http://dx.doi.org/10.1016/j.dsr.2013.12.008

into the Southern Ocean, where the sound channel axis is at the surface, the acoustic propagation is below the upper-ocean depths where most ocean warming has been reported.

The Appendix describes the 1960 experiment in detail, with the aim of establishing the accuracy of the 1960 travel time measurements. For the purposes of acoustic thermometry, the critical pieces of information are the accuracy of the time and position of the shots. Historical research has located the Ship′s Log and captain′s monthly "Report of Proceedings" to the Australian Department of the Navy, which describe how the explosive shots were deployed. The shots occurred at 3 am on 22 March 1960 local time about 175 km to the northwest of Cape Leeuwin. Positioning, timing, and other aspects of this study affecting the accuracy of measured and computed travel times are critical discussions for this paper.

The principal goal of the Perth-to-Bermuda acoustic propagation problem has been to find acoustic paths arriving at Bermuda that account for horizontal refraction by the ocean and that are not blocked by topographic features. The main ocean features affecting the refraction are the Antarctic Circumpolar Current (ACC) and the Agulhas Rings. If horizontal refraction is ignored, the WGS′84 geodesic is the obvious direct path (Fig. 2). However, as was pointed out by Munk et al. (1988), the sound speed variations of the ocean cause the paths to be refracted. Attempts to find paths in smoothed ocean atlases between the locations of the Perth shots and the Bermuda receiver that do not interact with the sea floor have been unsuccessful. If the horizontal refraction is accounted for, the paths were blocked by the African continent (Munk et al., 1988; Dushaw, 2008). By relying on acoustic interactions with the north side of Kerguelen Island and the north coast of Brazil, Heaney et al. (1991) obtained successful paths, however. While state-of-the-art for its time, the Heaney et al. (1991) solution necessarily employed environmental data with poor resolution by modern standards. Since acoustic refraction depends primarily on sound speed gradients, the Heaney et al. solution was not influenced by the sharper features of ocean variability. The present study adopted the same procedures as Heaney et al. (1991): first two-dimensional maps of acoustic mode phase speed were computed, and then rays were traced through these maps to obtain ray paths in latitude and longitude. These procedures were applied to recent high-resolution ocean state estimates and Smith and Sandwell (1997) sea-floor topography, however. This class of computational problem for long-range acoustic propagation has broad-ranging applications, such as monitoring for clandestine undersea atomic tests (de Groot-Hedlin, 2005; Prior et al., 2011) or remote determination of the properties of undersea earthquakes and other geophysical phenomena (de Groot-Hedlin et al., 2007; Talandier et al., 2006). Many of the antipodal-scale acoustic propagation issues addressed in this paper were introduced in the analysis of the HIFT acoustic data (McDonald et al., 1994; Chiu et al., 1994).

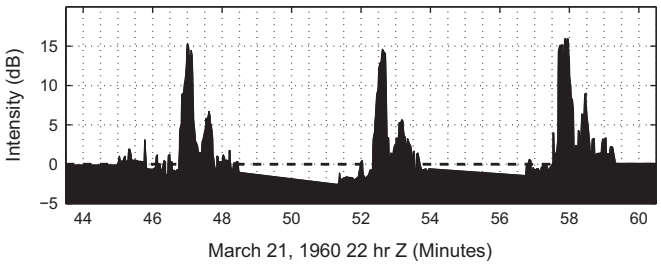

Fig. 1. Acoustic signals from the Perth shots that arrived at the Bermuda SOFAR Station′s Hydrophone Juliet. This hydrophone was located on the sound channel axis. The arrival coda from each shot consisted of a main arrival pulse of about 30-s duration and signal level 15 dB above the noise, followed by a weaker second arrival about 30 s later. The shot detonations occurred at 19 h 04 min 11 s, 19 h 09 min 43 s, and 19 h 15 min 07 s GMT, giving travel times of about 3 h 43 min. The spacing between the shot times is about 5 m 30 s. The graticule spacing along the abscissa is 30 s. These data were digitized from the original oscillogram figure of Shockley et al. (1982).

The first step of the present analysis was to determine if realistic ocean variability could refract acoustic paths sufficiently to arrive at Bermuda without interaction with the sea floor. No reliable solution was found, however, although the smaller-scale features of ocean variability substantially affected the acoustic propagation. It would have been more esthetic to obtain a solution that did not involve bathymetric interaction, but this did not prove possible. The influences of the sea floor on acoustic propagation were then modeled. Modeling the acoustic interaction with the sea floor required a number of assumptions about the acoustical interaction with the sea floor.

Section 2 describes how the nominal expectation of a −9 s travel time signal was obtained. The frequency spectrum of the shot signals, essential for determining the properties of acoustic propagation, is described in Section 3. Section 4 describes the ECCO2 state estimates and the calculation of mode-1 phase speeds, including the effects of a shoaling sea floor. In Section 5, the calculation of ray paths, with topographic features ignored, shows that the ocean-only influence on the paths is insufficient to refract the paths to Bermuda. The additional influence of topographic interaction on the ray paths is described in Section 6, showing that this additional influence accounts for the Bermuda arrivals. In Section 7, the calculation of the acoustic arrival patterns at Bermuda using the parabolic equation method is described. Computed arrival coda are obtained that are similar to the measured arrival coda. The uncertainties of the observations and the computations are summarized in Section 8. In Section 9,

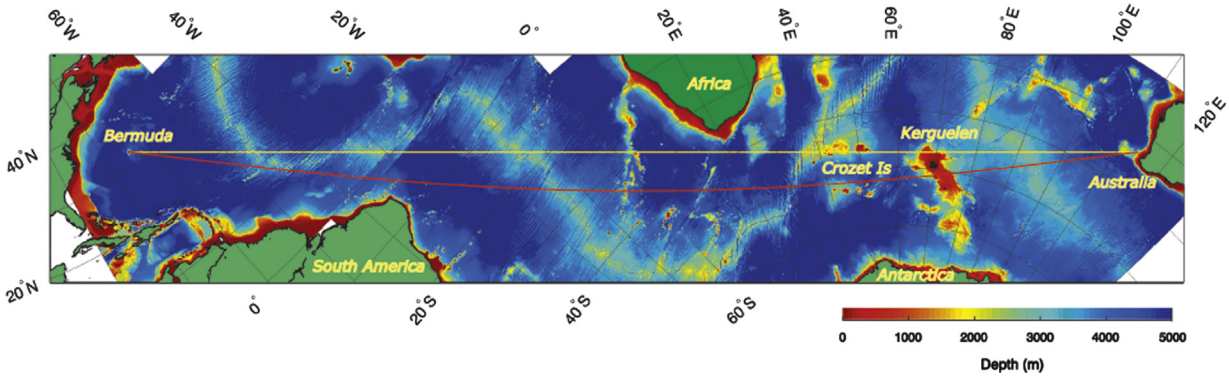

Fig. 2. Sea floor topography Smith and Sandwell (1997) (ver. 12.1) between the location of the shots off Perth, Australia (right) and Bermuda (left). The great circle route is indicated by the straight yellow line, while the WGS84 geodesic is indicated by the red line. Aside from the obvious continents, the main obstructions for the acoustic path were the Kerguelen Plateau and the Crozet Islands. With this oblique Mercator projection, the great circle route between the two points is a straight line with minimal mapping distortion about this line. (For interpretation of the references to color in this figure caption, the reader is referred to the web version of this paper.)

the theoretical caustic arrivals for antipodal arrivals described by Longuet-Higgins (1990) are briefly discussed in the context of the present results. Finally, Section 10 gives a concluding discussion.

2. A nominal estimate of the expected travel time change from a half-century of ocean warming

Obtaining a nominal estimate for the expected travel time change after a half century for the antipodal path is not a straightforward task, since any such estimate is fraught with approximations, caveats and nuances in interpretation. Nevertheless, such an exercise is worthwhile, since a nominal number of the right order of magnitude guides the analysis and the interpretation of the results. An alternate estimate of the expected warming along the acoustic path, computed from recent estimates of historical thermal anomalies by Levitus et al. (2012), is described in the Discussion section.

Munk and Forbes (1989), motivated by the 1960 antipodal transmission experiment, estimated warming of 5 m °C yr^{-1} near the sound channel axis, based on estimates of sea level rise by pelagic tide gauge measurements of 1–2 mm yr^{-1}. They assumed a conversion factor of 4 m s^{-1} per °C relating sound speed to temperature variations. Based on the estimates of Munk and Forbes, acoustic travel times over the 19.8 Mm path between Perth and Bermuda would decrease by 173 ms yr^{-1}, or a net decrease of 8.7 s after a half century. Warming causes sound speed to increase. The conversion factor is temperature dependent, however, and the temperatures near the sound channel axis range from about 2 °C near the surface in the Southern Ocean to about 11 °C at about 1200 m depth in the Sargasso Sea. The conversion factor therefore ranges from about 4.3 m s^{-1} per 1 °C in the Southern Ocean to 3.8 m s^{-1} per 1 °C in the Sargasso Sea, with an average over the antipodal path of about 4.2 m s^{-1} per 1 °C. Munk and Forbes (1989) point out the issue of the "noise" of decadal and mesoscale variability in attempting to extract the climatological trend. Nevertheless, after a half century the effects of a trend become substantive; Munk and Forbes (1989) estimated that the climatological signal in long-range acoustic measurements would become distinguished from normal geophysical noise after about a decade.

The nominal warming rate employed by Munk and Forbes (1989) is comparable to more recent observations of ocean warming. Common issues with such analyses are the underlying uncertainties and biases caused by the undersampling of the ocean and by the perennial sources of uncertainty and bias of diverse instrument types (Lyman et al., 2010). In addition, a common theme is that warming is not uniform, either spatially or with depth, with specific patterns indicated in the various ocean basins. Levitus et al. (2000, 2005) found an increase in upper ocean heat content in the Indian and Atlantic oceans equivalent to about 0.25 °C temperature rise in the upper 700 m since 1960. For this estimate, Levitus et al.'s results for the Atlantic and southern Indian oceans were combined using a 60–40 weighting, respectively. Temperature is derived from the heat content values using a crude estimate for the volume of water of the upper 700-m of the Atlantic and southern Indian Oceans and a nominal value for the specific heat of seawater. While this estimate is crude, more careful estimates, e.g., Lyman et al. (2010), obtain large uncertainties in the rate of warming.

Gille (2008) carefully examined long-term trends in heat content in the Southern Ocean derived from hydrographic data dating back to the 1930s. Gille (2008) found that "the upper 1000 m of the Southern Hemisphere ocean had warmed substantially [since the 1930s] at all depths." Between 30° and 50°S, Gille estimated a warming rate for the Southern Ocean between 300 and 1000 m depths of 0–20 m °C yr^{-1}. Uncertainties were large, but this estimated rate is comparable to Munk and Forbes's (1989) 5 m °C yr^{-1}.

For the purposes of the present analysis, the travel-time perturbation $\Delta\tau$ due to a sound-speed perturbation ΔC for a signal traveling a range R along the sound-channel axis is

$$\Delta\tau = -\frac{\Delta C}{C^2}R \tag{1}$$

or, using a sound speed–temperature conversion factor of 4.2 m s^{-1} per °C,

$$\Delta\tau = -\frac{4.2\Delta T}{C^2}R. \tag{2}$$

Using $\Delta T = 0.25$ °C as the net temperature change over the past half century, $C = 1485$ m s^{-1} as a nominal value for sound speed near the sound channel axis, and a range of 19,820 km, gives $\Delta\tau = -9.4$ s. The conversion rate between sound speed and temperature is, in the present analysis, more properly determined by the rate of change of group speeds of acoustic modes with temperature. This rate of change is dependent on the depth-dependent form of the acoustic modes, which are centered on the sound channel axis, and the profile of temperature change. In any case, the results of this crude calculation are used as the basis for the nominal expectation that acoustic travel times between Perth and Bermuda may have decreased by about 9 s as a consequence of oceanic warming trends.

3. The frequency spectrum of the explosive shots

One goal of this analysis was to compute the expected arrival coda at Bermuda in detail for comparison with the 1960 measurements. Such a comparison is required to accurately determine the present-day travel time relative to the 1960 travel time. This calculation requires an estimate for the frequency spectrum of

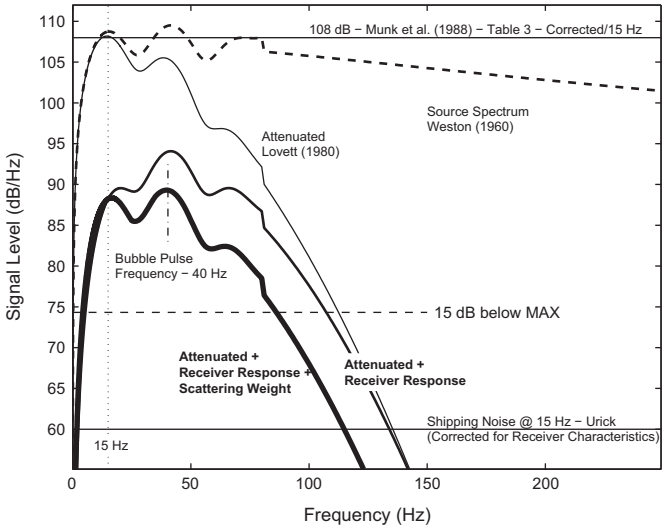

Fig. 3. Calculation of the frequency spectrum of the signal arriving at Bermuda. The intensity calculation of Munk et al. (1988) was used to set the absolute intensity level. The initial source spectrum was calculated assuming that 300-lb TNT was detonated at 4800 ft (800 ftm) depth (Weston, 1960) (dashed line). The frequency dependence of attenuation by seawater was accounted for following Lovett (1980) (light line). The response characteristics of the Bermuda receiver reduced the recorded lower-frequency sound levels (medium line). Finally, the frequency dependence of the topographic scattering of the sound reduced the higher-frequency sound levels (heavy line). The recorded signals (Fig. 1) peaked at about 15 dB/Hz above the noise, hence this noise level is indicated. After correcting for the receiver response, the shipping noise at 15 Hz was about 60 dB/Hz (Urick, 1983), however. The different noise levels suggest the signal intensity lost by topographic interaction. Intensity units are more properly dB/Hz Re 1 μPa at 1 yd, abbreviated to dB/Hz.

the pulse as it arrived at Bermuda, since the properties of acoustic modes depend on frequency.

The frequency spectrum and peak intensity of sound generated by an explosive shot can be accurately calculated, given the depth and yield of the explosion (Fig. 3) (Weston, 1960; Urick, 1983). The charges were designed to detonate at 800 ftm, although in practice this depth was not precise (Appendix). The yield of the depth charges was equivalent to 300-lb TNT (Appendix). Following Weston (1960), the first three peaks in the spectrum from bubble frequencies are given in Fig. 3, while at higher frequencies an asymptotic form for the spectrum was used. The dominant bubble frequency is 40 Hz.

Munk et al. (1988) (their Table 3) calculated the peak intensity at 15 Hz of the acoustic pulses arriving at Bermuda as 108 dB/Hz Re 1 μPa at 1 yd (abbreviated to "108 dB"), assuming 300-lb yield and 3000-ft detonation depth, and this value will be adopted to set the overall intensity of the spectrum. This calculation included a small loss of 1 dB by attenuation (Lovett, 1980), the loss of 146 dB due to signal spreading over 20,000 km range (approximating spherical spreading to 10 km, cylindrical spreading to 20,000 km, and time spreading of the detonation time scale to the 20 s recorded pulse duration), and a gain of 20 dB from antipodal focussing.

The shape of the spectrum of the recorded signal is affected by the frequency-dependent nature of the acoustic propagation and the frequency response properties of the Bermuda receiver. The frequency dependence of seawater attenuation was calculated following Lovett (1980). The Bermuda receiver response (peaked at 150 Hz with a 6 dB/octave drop-off to both sides Munk et al., 1988) reduces the recorded lower frequency sound levels. Finally, the necessary acoustic scattering from topographic features is weaker for higher frequencies (see Section 6), so the intensities of higher frequencies are further reduced. Combining all these contributions, the broad-band frequency spectrum of the recorded signals was estimated to span 10–85 Hz and peak at about 89 dB at around 40 Hz.

Munk et al. (1988) calculated a dominant bubble frequency of 15-Hz, assuming an acoustic source with 300-lb yield and 300-ft [sic] detonation depth. This frequency was also used by Heaney et al. (1991) for their study. The spectrum computed for 4800-ft depth has greater intensities at higher frequencies, however. The analysis below also initially assumed an acoustic frequency of 15-Hz for consistency with this previous work. The broadband nature of the acoustic pulses is an aspect of the propagation problem that must be taken into account, however.

After correcting for the receiver response, the noise at 15 Hz, mainly due to shipping, was about 60 dB (Urick, 1983; Munk et al., 1988), so the maximum intensity of the estimated spectrum was about 29 dB above the noise floor. The recorded pulse intensities were only 15 dB above the noise (Fig. 1), however. As will be discussed below, the difference between the expected and observed signal levels is an indication of the additional loss of signal intensity resulting from topographic interaction.

4. The ECCO2 ocean state estimates and acoustic mode properties

4.1. Sound speed derived from ECCO2 state estimates

In this study we used two data-constrained, time-evolving, eddy-permitting, global ocean and sea ice state estimates provided by the "Estimating the Circulation and Climate of the Ocean, Phase II" (ECCO2) project (Menemenlis et al., 2008). These state estimates were the best available when we began this study. The first ECCO2 state estimate, hereinafter called "cube78", is a partially constrained simulation, whereby a small number (80) of model parameters have been adjusted using Green's function approach (Menemenlis et al., 2005a). The second ECCO2 state estimate, hereinafter called "iter22", is a more fully constrained solution, whereby a much larger number (2×10^6) of model parameters have been adjusted using the adjoint method (Wunsch et al., 2009). The cube78 and iter22 solutions were obtained on a cube sphere grid with 18-km horizontal grid spacing and 50 vertical levels (Menemenlis et al., 2005b). Monthly mean temperature and salinity profiles from the cube78 solution were provided on a 1/4° global grid for the period 1992–2006. Three-day-mean temperature and salinity profiles from the iter22 solution were provided on the same 1/4° grid for the period 1 January 2004 to 30 April 2005. One notable difference between the two estimates is that the Agulhas Rings are more irregular and have weaker sound speed signatures in the iter22 solution. This difference is attributed to the somewhat more viscous and diffusive model configuration that was used to integrate the iter22 solution. The procedures for calculating sound speed profiles from the state estimates are straightforward (Dushaw et al., 2009): (1) in situ temperature is calculated from estimated potential temperature, (2) those profiles are combined with model salinity profiles to calculate pressure, and (3) temperature, salinity, and pressure are then used to obtain sound speed from the standard equations for sound speed in sea water (Del Grosso, 1974; Dushaw et al., 1993, 2013) (Figs. 4 and 5). Sound speed fields constructed from the ECCO2 state estimates appear to have fairly accurate acoustical properties, a notable achievement (Dushaw et al., 2013). Evaluation of cube78 and iter22 against 2004 Argo profiling float data collected along a 1000-km swath centered along the Perth-to-Bermuda refracted geodesics shows a positive sound speed velocity bias of 0.6 m/s for cube78 and 0.2 m/s for iter22 when integrated along the sound channel axis. Corresponding travel time biases are −5 s and −2 s for cube 78 and iter22, respectively.

4.2. Acoustic modes

The acoustic mode functions, phase and group speeds for the world's oceans were calculated using the well-established KRAKEN code (Porter and Reiss, 1985; Jensen et al., 1994) (Figs. 6 and 7). This computationally intensive task involved solving the acoustic eigenvalue problem at each of the 1440 × 720 points of the 1/4° grid for each of the monthly means of cube78 and three-day averages of iter22. The effect of the curved earth on subsurface acoustic propagation is accounted for by applying the flat-earth transformation to the sound speed profiles (Aki and Richards, 1980). Without this correction computed antipodal travel times are erroneously large by 2 s. The mode properties were calculated using 15, 25, 35, 50, 75, and 100-Hz acoustic frequencies. The mode properties were first computed by ignoring the sea floor, with the ocean taken everywhere to be 5-km deep, and then by employing a simple model for ocean bottom sound speed. The effects of the ocean alone on the acoustic ray paths could then be determined.

4.3. A simple model for sound speed below the sea floor

The refractive effects caused by acoustic interaction with shoaling topography were examined by Munk and Zachariasen (1991) in an attempt to resolve the Bermuda arrival problem. Shoaling topography increases the mode phase speeds, hence tends to refract away acoustic modes. The influence of the African continental shelf on acoustic propagation is to refract rays away from Africa, which is the opposite effect of what is required to get rays to bend toward Bermuda.

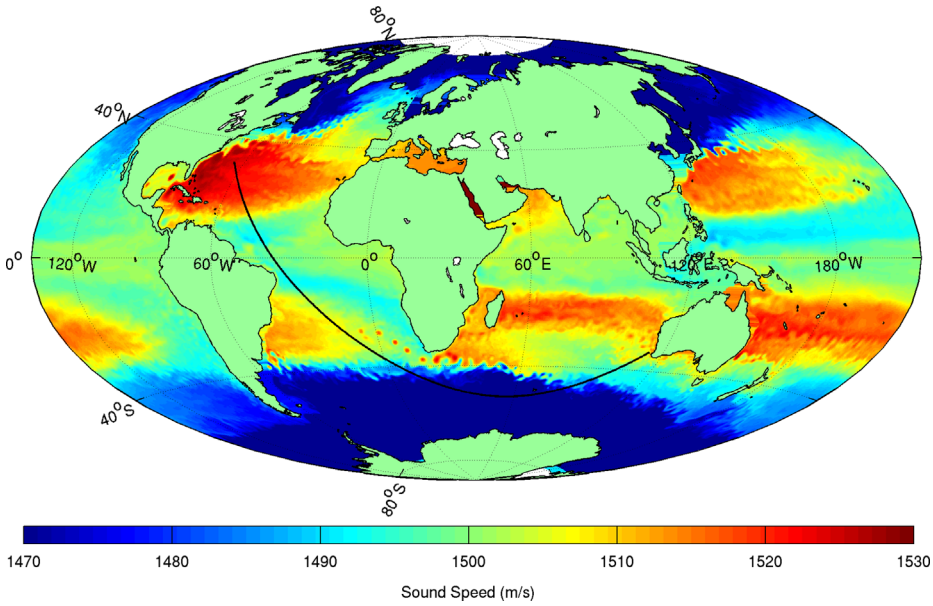

Fig. 4. Sound speed at 300 m depth derived from the ECCO2 cube78 state estimate for August 1993. The WGS84 geodesic path between the location of the Perth shots and the Bermuda SOFAR station receivers is indicated. The notable features, insofar as antipodal acoustic propagation is concerned, are the sharp and filamental nature of the Antarctic Circumpolar Current and the regular spinoff of intense Agulhas rings from the southern tip of Africa into the South Atlantic. Hammer-Aitoff projection.

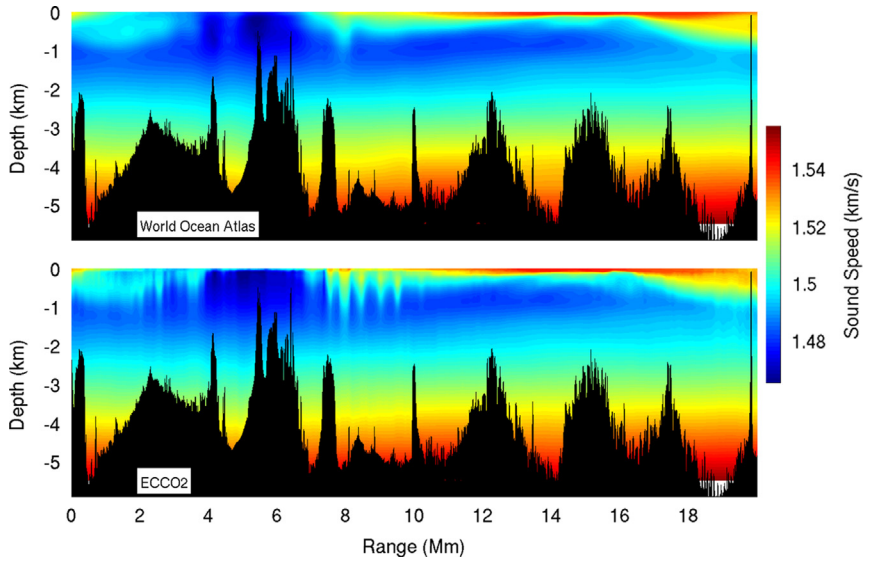

Fig. 5. Sound speed sections along an acoustic path between Perth and Bermuda computed using the 2009 World Ocean Atlas (top) and the ECCO2 cube78 state estimate (bottom) for February 1997. At midlatitudes and the tropics the sound channel axis is near 1000 m depth, while south of the ACC it is at the surface. The undulations in sound speed at around 8 Mm range correspond to a sequence of Agulhas rings in the South Atlantic. The Kerguelen Plateau is at about 6-Mm range, and the Bermuda Rise is apparent at the far right.

The nature of the sea floor will influence the phase speeds of the acoustic modes (Hamilton, 1980, 1987). The sediment layer near Cape Agulhas and many regions of the world′s oceans is several kilometers thick (Divins, 2003), hence it is effectively infinitely thick insofar as its influence on low-frequency acoustic modes is concerned. Sometimes, the sound speed of the sediment just below the sea floor is significantly less than the ocean sound speed. In this situation, as acoustic signals approach a shoaling sea floor, mode phase speeds may first decrease when mode functions begin to interact with the sea floor, but then increase with further shoaling. The mode properties depend on the nature of the ocean bottom (e.g., clay, gravel, limestone, or basalt) and sound speed at the ocean–sea floor interface (Jensen et al., 1994). Further, in many cases the ocean bottom supports both compressional and shear waves, both of which become relevant to accurately computing acoustic interactions with the sea floor. Alas, for most of the ocean sea floor detailed geophysical and sound speed data are not readily available. In the absence of worldwide data for the sound speed properties within the sediment, the calculations here will employ a simple model for sound speed within the sediment: beginning with the oceanic value for sound speed at the sea floor, sound speed increases linearly with depth at a rate of 100 m s^{-1} per 600 m. With this rapid increase in sound speed with depth and for acoustic frequencies near 40 Hz, the mode functions do not penetrate far into the sediment. For similar reasons of expediency, the increased attenuation caused by acoustic interaction with, or scattering from, the sea floor is ignored; the frequency-dependent details of this attenuation are beyond the scope of this paper. The aims of this model are simply to account for the

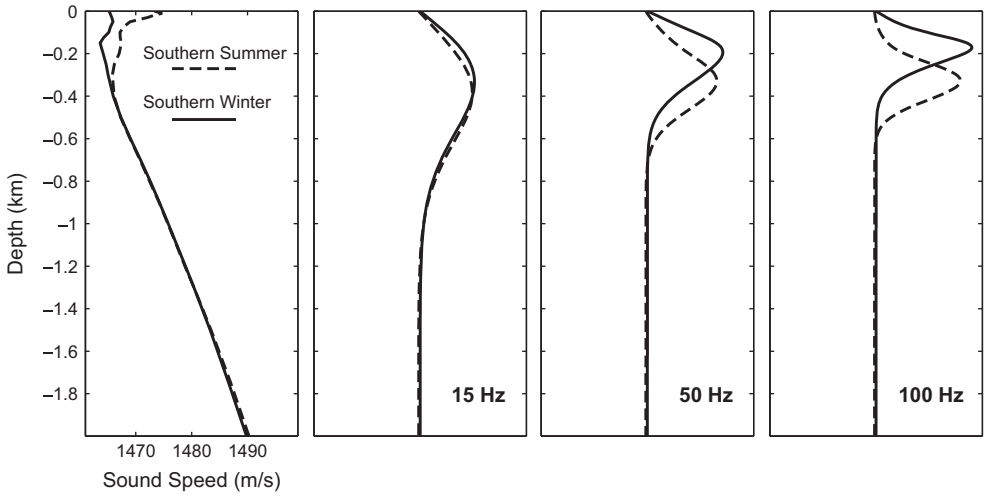

Fig. 6. Acoustic modes at 15, 50, and 100 Hz for the region of Kerguelen derived from an ECCO2 state estimate. Modes at higher frequency are shallower, hence less likely to interact with topographic features. The shapes and depth ranges of the modes vary seasonally. The modes are shallower in southern winter with the absence of a warm surface mixed layer.

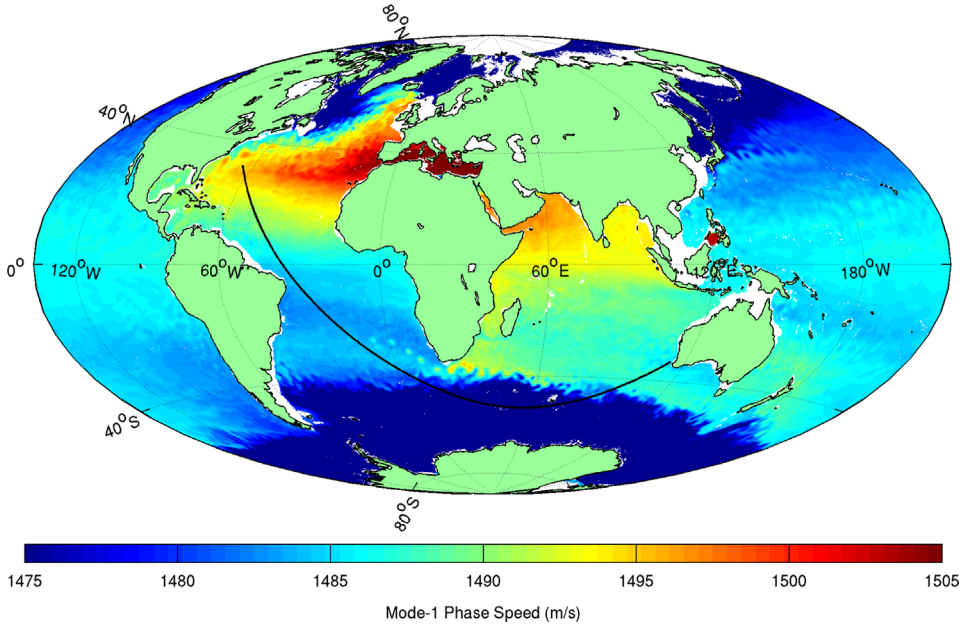

Fig. 7. Acoustic mode-1 phase speed at 15 Hz derived from the ECCO2 cube78 state estimate for August 1993. The WGS84 geodesic path between the location of the Perth shots and the Bermuda SOFAR station receivers is indicated. The phase speed is a variable strongly dependent on ocean temperature; mode-1 phase speed variations follow those of ocean temperature near the sound channel axis. Hammer-Aitoff projection.

increase in mode phase speeds near shallow topographic features in order to allow the refractive influences of such features to be roughly accounted for, or to allow shoaling features to block or terminate acoustic signals in an approximate way. Computations of accurate, frequency-dependent, absolute sound levels are not necessary to address the main aims of the present study.

4.4. Nested resolutions

The sea floor topography employed for the acoustic computations was the Smith–Sandwell 1′ resolution global topography (ver. 12.1) (Smith and Sandwell, 1997). The resolution of this data base is considerably finer than the 18-km grid of the ECCO2 state estimates. Solving the acoustic mode problem for the world's oceans on a 1′ grid is a challenging computational problem. For this reason, following Heaney et al. (1991), a nested approach was used, so that in shallower regions of interest (Kerguelen Plateau, the Crozets, the South African continental shelf, the east coast of Brazil) the modes were calculated on a 1′ grid, while over most of the ocean where the water depth is too deep to affect the lowest acoustic modes, the modes were calculated on a 1/4° grid (Figs. 8 and 9). As is illustrated in Fig. 8, the variations in mode phase speed caused by topographic features are strongly frequency dependent. In the Southern Ocean where the sound channel axis is at the surface, higher-frequency modes are shallower (Fig. 6), hence they have a greater chance of avoiding the influences of shoaling topography. As a result, the cross sections for scattering from topographic features are much weaker for higher-frequency modes.

Ray tracing employed an integration step size of 2.72 s (4 km) for most of the ocean. The step size was reduced to 0.136 s (200 m) within shallow regions to accurately compute ray interaction with fine-scale topographic features. The horizontal grid spacing of Smith–Sandwell topography is a little less than 2 km. Topography was estimated for points on the integrated ray paths by two dimensional linear interpolation.

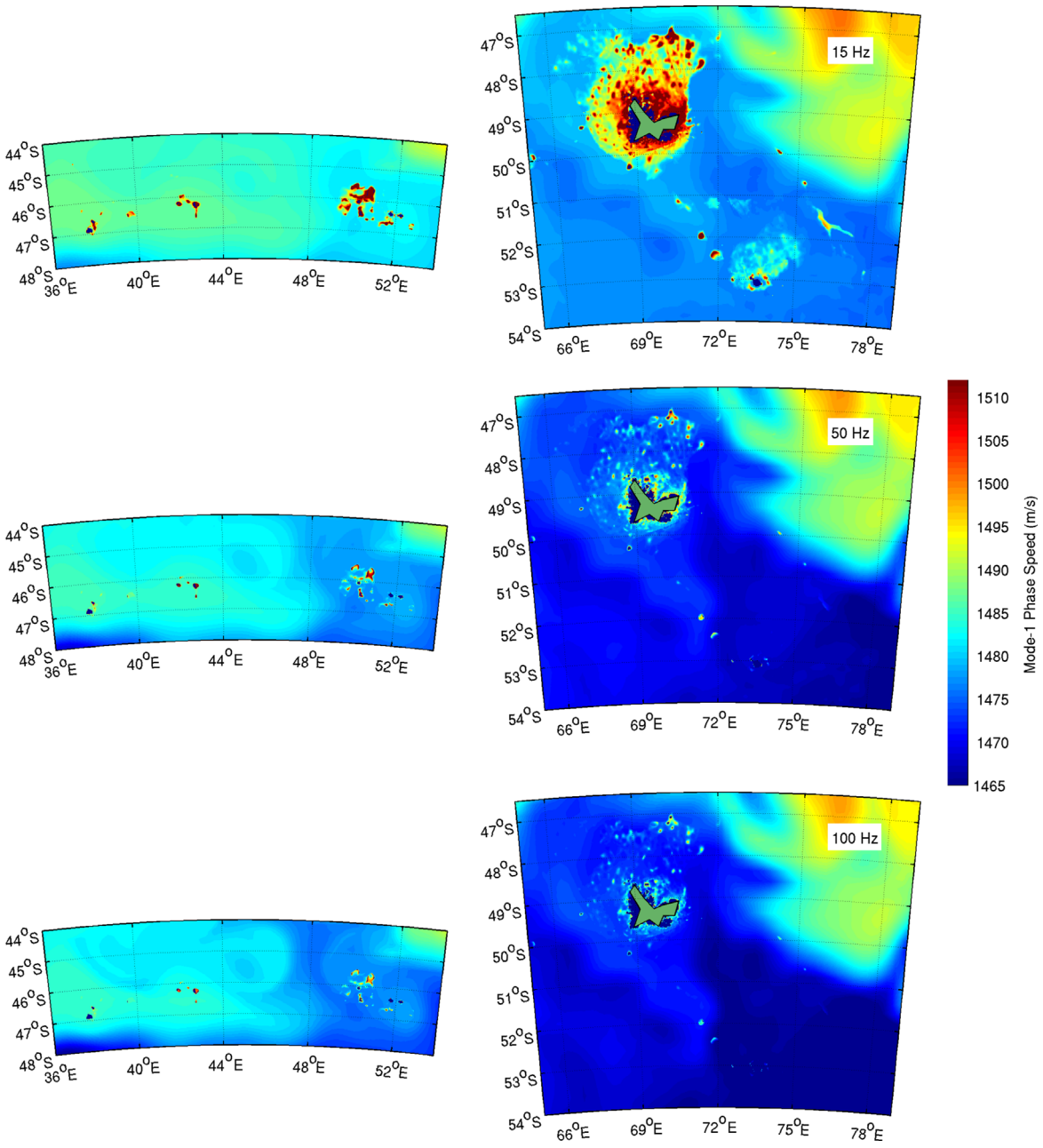

Fig. 8. Acoustic mode-1 phase speed at 15, 50, and 100 Hz for the areas around the Crozet (left) and Kerguelen (right) Islands derived from the ECCO2 cube78 state estimate for August 1993.

4.5. Mode-1 phase speeds of the world's oceans

The variability of mode-1 phase speeds obtained for the world's oceans is directly related to the ocean temperature variability near the sound channel axis. The effects of variations in salinity are minimal (Dushaw et al., 2009). At midlatitudes and the tropics the sound channel axis is near 1000 m depth, while south of the ACC it is at the surface (Fig. 6). The variations of mode phase speed over time reflect the oceanographic signals that would be measured by acoustic tomography in any region of the globe, at least for acoustic propagation along the sound channel axis. For example, the phase speed variations apparent in the equatorial Eastern Pacific reflect El Niño-La Niña variability. For the purposes of acoustic propagation between Perth and Bermuda, the ACC appears in mode phase speed as a sharp front and a turbulent environment, while the Agulhas Rings appear as "lenses" of large phase speed. For acoustic measurements that integrate over long distances, the contribution of individual mesoscale features to travel time variations is greatly reduced. The maps of mode phase speed obtained from each ECCO2 model snapshot are all that are needed to calculate the paths and travel times of acoustic propagation by ray tracing.

5. Ray tracing in ECCO2 state estimates: without topographic interaction

By ray tracing through a realistic ocean environment, rather than a highly smoothed ocean atlas, and excluding the effects of topographic features on the mode properties, we seek to determine whether the realistic refractive effects of the ocean alone can induce acoustic paths between Perth and Bermuda. Following Heaney et al. (1991) and Jensen et al. (1994), procedures for ray tracing over

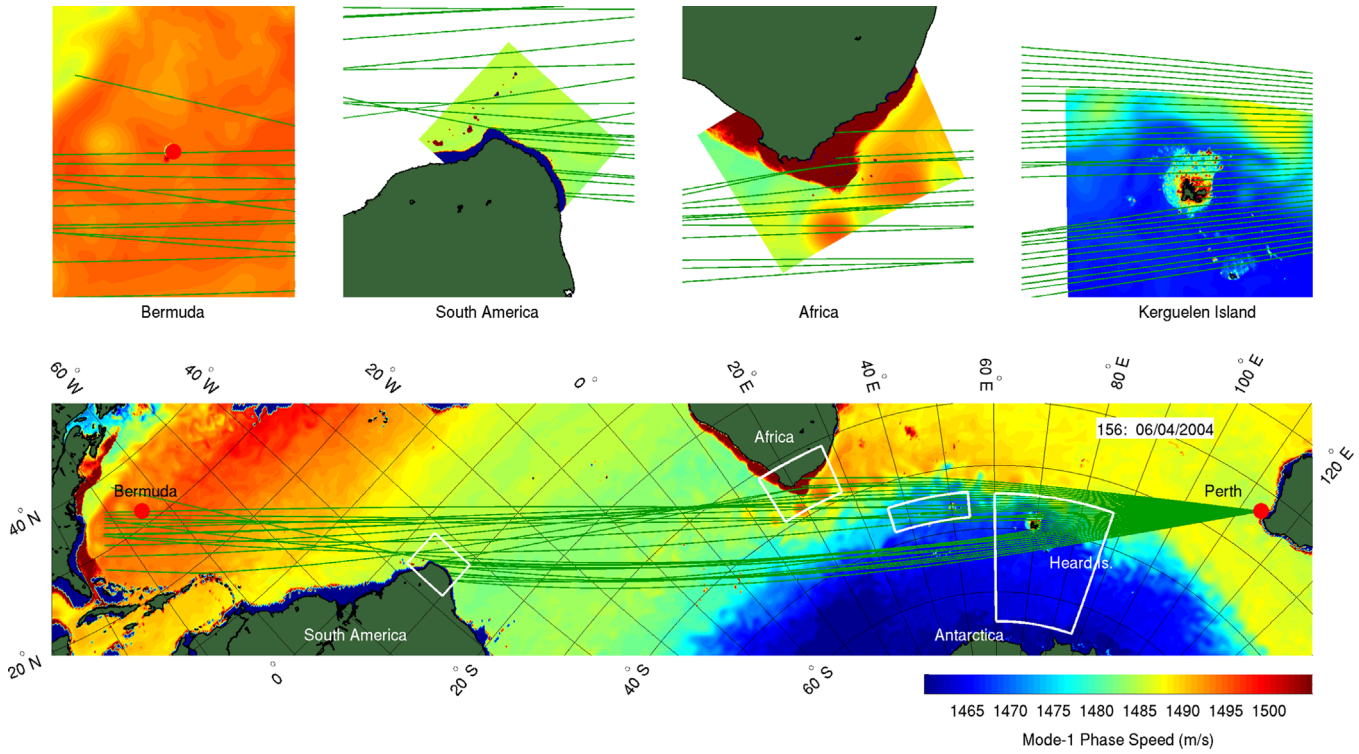

Fig. 9. A fan of rays is traced from the source location near Perth. Ray trajectories were determined by oceanic refraction and scattering from topographic features. The mapped colors indicate mode-1 phase speed for 15-Hz acoustic frequency derived from the cube78 solution for April 2004. Most rays either terminate at continental boundaries or pass south of Bermuda. Most often rays arriving at Bermuda have scattered from topographic features in some way. The left panels show topographic interaction in detail: Kerguelen and the Crozet Islands are near perfect scatterers, the African continental shelf is a near perfect refractor, while the Brazilian continental shelf is a near perfect reflector. (For interpretation of the references to color in this figure caption, the reader is referred to the web version of this paper.)

antipodal distances using a two-dimensional field of mode-1 phase speed were previously developed using the World Ocean Atlas (WOA) (Dushaw, 2008). The ray equations were described by Munk et al. (1988), following Aki and Richards (1980). These coupled differential equations, integrated using the fourth-order Runge–Kutta method (Press et al., 1992), are essentially those used to derive geodesics on the ellipsoidal earth, generalized to include the effects of horizontal refraction. Travel times are obtained by integrating the mode group speed over the acoustic paths (Jensen et al., 1994).

The accuracy of the ray calculations was verified by using them to solve for unrefracted geodesics, which can be tested against established solutions (Vincenty, 1975). Such solutions are obtained by using a constant value for sound speed. The range of the antipodal distance obtained by ray tracing was in error by 35 m, corresponding to an insignificant travel time error of 23 ms.

For each ECCO2 snapshot, a dense fan of rays was traced, sweeping over azimuthal angles, to determine the nature of the acoustic refraction and search for rays arriving at Bermuda by brute force. Ocean variability caused the acoustic paths to meander and deviate considerably from the geodesic. There was no single stable ray path or set of ray paths. The refraction of the ray paths is governed by the horizontal gradient of phase speed, but no single oceanographic feature had a strong effect on the ray paths. For example, the Agulhas Rings did not by themselves strongly refract the paths. Rather, the fate of any particular ray depended on the accumulated effect of ocean variability. The coasts of Brazil and South Africa form a narrow aperture for rays to propagate into the North Atlantic.

In most cases, the acoustic paths arrived to the south of Bermuda. Bermuda is in the acoustic shadow of Africa from Perth. The mean and RMS of the distances of the paths from their closest approach to Bermuda were 135 ± 52 km. This distance is considerably less than the 400-km distance obtained using the WOA (Dushaw, 2008). There were several instances in which paths successfully arrived at Bermuda, however. Such rays typically were refracted by the ACC such that they then passed through the northern portion of a sequence of Agulhas rings in the South Atlantic, each ring contributing a refractive influence northward. Statistically, the chance of an acoustic path arriving at Bermuda was a few percent. The distance of the arrivals from Bermuda was a smooth, rather than random, function of initial azimuthal angle of the rays, that is, the traced rays were not chaotic. The paths arriving nearest to Bermuda passed near (either north or south of) the Crozet Islands and well to the south of Cape Agulhas.

Excluding topographic interaction gave the unacceptable result that the acoustic paths usually missed Bermuda. One conclusion might be that the 1960 experiment occurred at one of those infrequent times for which a successful path was possible. Other possibilities are that the acoustic scattering by internal waves induced horizontal diffusion of acoustic energy (Munk et al., 1988) such that acoustic energy arrived at Bermuda (equivalent mesoscale diffusion, also discussed by Munk et al., 1988, is explicitly accounted for in the ECCO2 ray tracing computations), or that the ocean's state has changed over the past 50 years such that acoustic arrivals at Bermuda are no longer possible. Perhaps if the 1960 experiment was repeated today, it would fail. These unlikely scenarios aside, more satisfactory results were obtained by accounting for the influence of the sea floor.

6. Ray tracing in ECCO2 state estimates: with topographic interaction

Ray tracing through the ECCO2 30- or 3-day time averages of mode-1 phase speed, including the complication of topographic interaction, usually resulted in two groups of paths between Perth and Bermuda (Figs. 9 and 10). The most direct path was that in

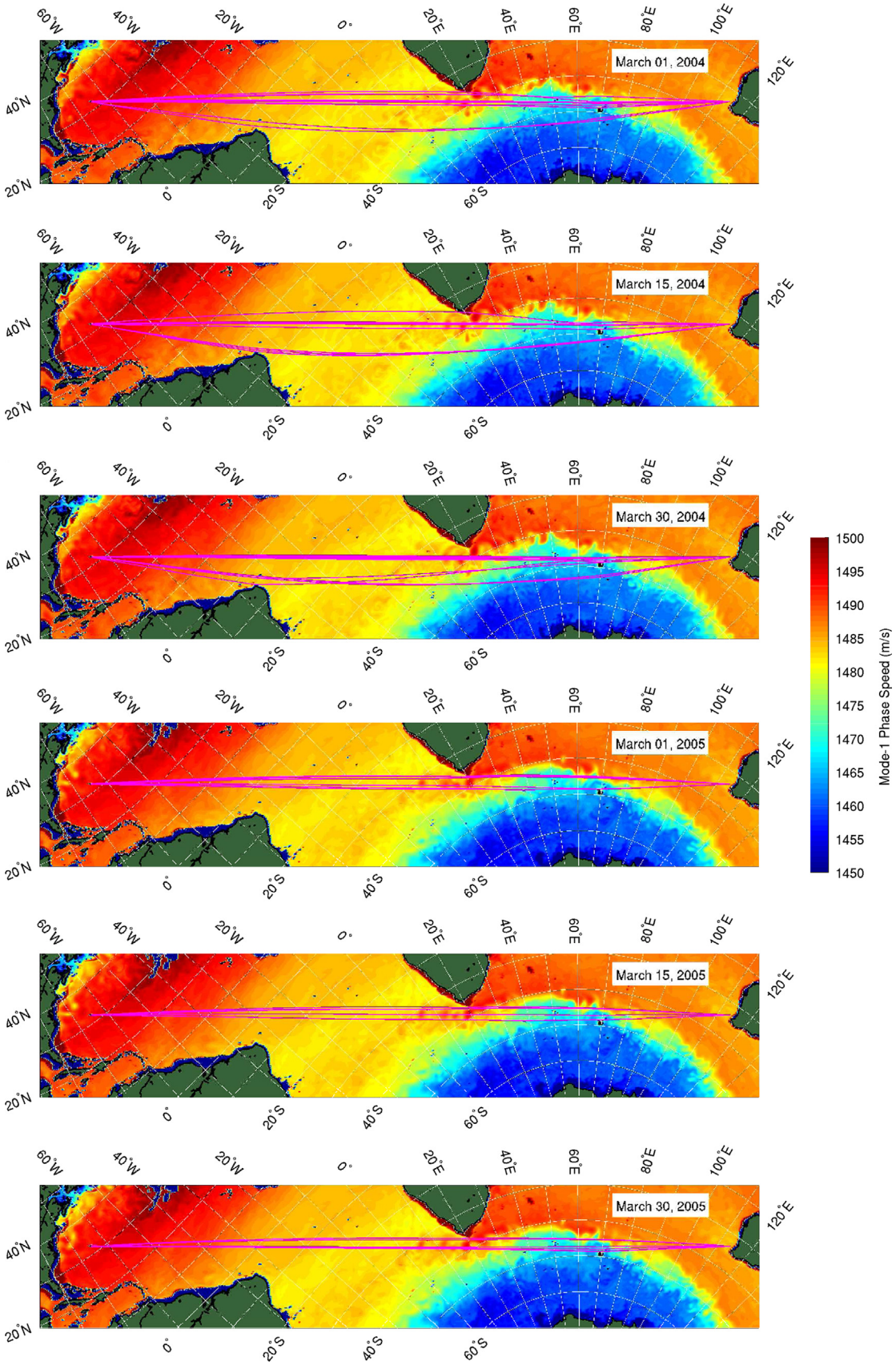

Fig. 10. Ray paths between the location of the Perth shots and the Bermuda receiving hydrophone obtained for a selection of ECCO2 state estimates for the times indicated at the upper right of each panel. The mapped colors indicate mode-1 phase speed for 25-Hz acoustic frequency. The complicated environment of the Antarctic circumpolar front and Agulhas Rings are the dominant influences on the ray paths. The ray paths scintillate in response to the changing ocean conditions, but ocean variability alone is rarely sufficient to refract the rays such that they arrive at Bermuda. In the absence of topographic interaction, most rays pass to the south of Bermuda. (For interpretation of the references to color in this figure caption, the reader is referred to the web version of this paper.)

which the rays slightly scatter from seamounts near Kerguelen and the Crozets, while a secondary path passed near the Brazilian coast. Similar paths were obtained by Heaney et al. (1991). For the dense set of ray azimuthal angles employed (2125 rays were traced between 224° and 241° at 0.008° intervals) and at lower acoustic frequencies, a dozen or so individual rays to Bermuda were obtained with each ECCO2 time average. The ray tracing results shown in Fig. 9 illustrate three distinct mechanisms for how the ray paths interacted with topography: scattering from sea mounts near Kerguelen and the Crozets, refraction from a gentle continental slope near South Africa, and reflection from a steep continental slope near Brazil. As discussed above, the refractive effects of the realistic ocean caused rays to arrive significantly closer to Bermuda than was obtained from a smoothed ocean. In a realistic ocean, the topographic scattering required to redirect rays towards Bermuda is minimal.

The rays to Bermuda allow the mode-1 travel times associated with the acoustic pulses to be computed. This computation assumes adiabatic modes, wherein acoustic energy is not exchanged between modes, and requires a consideration of arrival intensity. In the next section, the complete arrival coda are computed, giving more accurate results for the computed travel times of the explosive source signals. The time series of mode-1 travel times shows that the variability of the travel times, caused by the movement of fronts, the mesoscale, or other variability, is surprisingly small.

6.1. Arrival intensity

The problem of estimating travel times from the ray tracing is linked to the problem of estimating amplitude, since the travel time is determined by the signals that have the dominant intensity at Bermuda. A lone ray arriving at Bermuda after passing near an isolated seamount is inconsequential; we seek the travel time associated with the dominant ray arrivals. A notional estimate of the amplitudes of these paths was obtained by using the ray density at the receiver to estimate relative amplitude (Fig. 11). The several arrivals at Bermuda (indicated in the inset of Fig. 11) were combined using a Gaussian weighting with 15-km width. Two wavefronts were obtained, one wavefront arising from a group of rays originating from the Crozets/Kerguelen, the other from the coast of Brazil. The travel times of the several rays associated with either of these ray groups are similar; the associated range is also obtained, of course. The travel times and relative amplitudes of these two arrivals were consistent with the measured doublet arrival patterns of Fig. 1, with the group of rays passing near Brazil arriving about 30 s later with weaker amplitude. As Munk et al. (1988) observed, the second pulse arrival is delayed not by a longer path, but by the slower sound speed encountered on the more southerly path; the ranges associated with these two antipodal ray groups are similar. For example, 11 rays were obtained for the 13–15 March 2004 iter22 time-average. Of these, seven were associated with the northerly path with mean and RMS range 19,825 $\pm$ 5 km and travel time 13,380 $\pm$ 1 s, while four were associated with the southerly path with range 19,824 $\pm$ 3 km and travel time 13,409 $\pm$ 17 s.

In 1960 the scientists conducting this experiment were puzzled by the weak arrivals at Bermuda (Appendix). The acoustic signal that avoided topographic interaction to arrive 135 km to the south of Bermuda was estimated by ray density to be about 30 dB more intense than the signal at Bermuda. The reason for the weak Bermuda arrivals is now evident.

The nature of this ray tracing problem is frequency dependent. As described above, the scattering strength of the Southern Ocean seamounts, or acoustic cross section, is greatly reduced for higher frequencies. Since the higher frequencies did not scatter well from the Kerguelen/Crozets seamounts, the intensity for these frequencies arriving at Bermuda was greatly reduced. Ray tracing was therefore repeated using 15, 25, 35, 50, 75, and 100-Hz acoustic frequencies, with the relative intensities at these frequencies determined by ray density. The overall effect of these phenomena on the acoustic spectrum of sound arriving at Bermuda was to reduce the intensities of the higher frequencies, as introduced in Section 3 (Fig. 3).

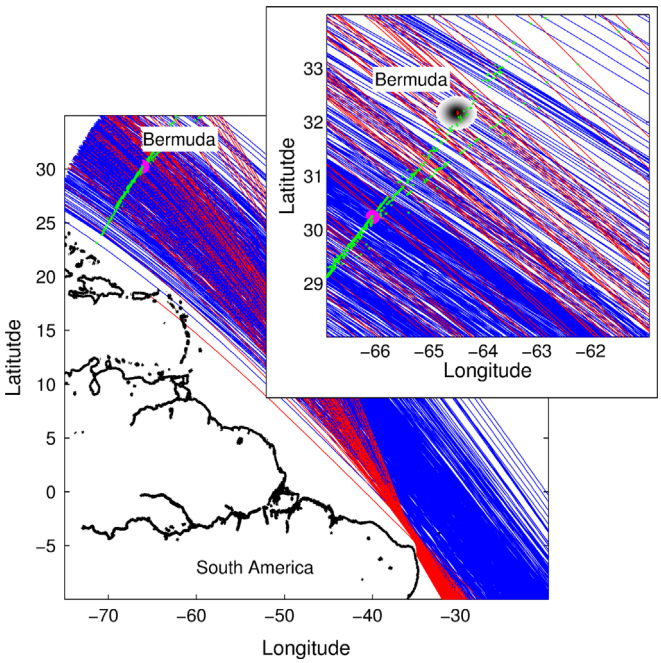

Fig. 11. A dense fan of rays is used to approximate arrival intensity by ray density. Scattering from small-scale topographic features usually allows rays to arrive at Bermuda. Rays noted in red have passed near the coast of Brazil. The inset panel details the region of Bermuda with the green dots along the ray paths indicating a wave front, defined by points of equal travel time. Rays also reflect or are scattered from the coast of Brazil forming a second wave front that arrives 30 s later. These rays were traced using mode phase speeds computed at 15-Hz frequency. At higher frequencies, the topographic scattering is weaker and the density of rays arriving at Bermuda is less. The direct, non-topographic interacting rays arrive a few hundred kilometers south of Bermuda (purple dot), with much greater ray density. (For interpretation of the references to color in this figure caption, the reader is referred to the web version of this paper.)

6.2. Time series of travel times

Mode-1 travel times for the acoustic arrival pulse were computed by combining the travel times of the individual ray paths by Gaussian weighting as described above for each of the ECCO2 time averages. Time series of mode-1 travel times for the first wavefront arrival were obtained for each of the 15, 25, 35, 50, 75, and 100-Hz frequencies (Fig. 12). As discussed above the higher frequencies had less chance of scattering towards Bermuda, so the time series at higher frequencies are noisier and have frequent gaps. Travel time had little dependence on frequency otherwise. The 15-year cube78 time series of 15-Hz mode-1 travel time had mean and RMS of 13,375 + 0.9 $\pm$ 2.6 s, while the time series derived from the first year of the iter22 estimates had mean and RMS travel time of 13,375 + 2.7 $\pm$ 1.8 s. Based on the small ECCO2 travel time variability, we make the conjecture that in the true ocean travel times of antipodal acoustic signals have remarkably little variation.

The mode-1 travel times in 2005 from the iter22 ECCO2 solution (Fig. 12) decreased by about 10 s. This travel time shift is associated with ray path solutions with a more northerly route (Fig. 10, lower three panels). The travel time decrease in this case is not caused by warming, but by the route through warmer regions.

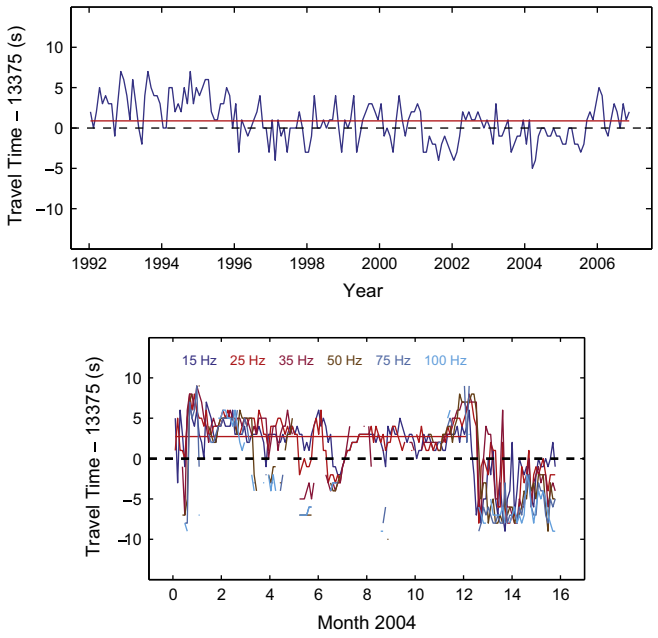

Fig. 12. Top: Time series of mode-1 travel times for 15-Hz frequency for the 15-yr cube78 state estimate. The mean travel time is indicated by the red line. Bottom: Time series of mode-1 travel times for the 15, 25, 35, 50, 75, and 100-Hz frequencies for the 16-mo iter22 state estimate. The shift in travel times at the start of 2005 corresponds to a northward shift in the ray paths arriving at Bermuda (cf. Fig. 10). The travel time of antipodal acoustic propagation has surprisingly little variation within the ECCO2 state estimates, and travel time is frequency independent. For higher frequencies, often no successful ray paths to Bermuda were obtained, as indicated by frequent gaps in the time series. (For interpretation of the references to color in this figure caption, the reader is referred to the web version of this paper.)

These solutions do not include a second arrival from the coast of Brazil, hence they are inconsistent with the 1960 observations. Further, none of the monthly-mean time averages from the 15-yr cube78 solution obtained ray paths of this type. The change in ray path solutions was traced back to a significant, and unrealistic, change in how the iter22 solution was characterizing the sound speed gradients within the ACC (Fig. 13). As the iter22 solution evolved, the higher diffusivity and viscosity of this adjoint-based solution eroded many of the small-scale features (eddies and meanders) that were present in the initial conditions, causing the ACC variability to become more monolithic. We therefore discount the 2005 travel times as having been adversely affected by unphysical artifacts of the ECCO2 state estimates.

The stability of mode-1 travel times over time derived from the ECCO2 estimates is an important result, since it means that the 1960 measurements, which occurred at essentially a single time, were not unduly influenced by oceanic variability. The geophysical variability represents a travel time uncertainty for the 1960 measurements, if we interpret them as a measure of the ocean climate in 1960.

7. Travel time comparisons 1960, 2004: computing arrival coda

While the mode-1 travel times have been computed, it is not obvious how this travel time should be compared to the recorded data (Fig. 1). Further, such travel times assume the adiabatic approximation (Heaney et al., 1991), wherein acoustic energy is not transferred between modes. As shown by Shang et al. (1994) and McDonald et al. (1994) in their analysis of HIFT data, the acoustic modes do not propagate adiabatically. In this section, the complete arrival coda are computed for direct comparison to the observed coda. This comparison gives an unambiguous comparison of the travel times derived from the ECCO2 state estimates to the observations.

7.1. Single sound speed section

To illustrate the various effects of ocean variability, frequency, and topography on the nature of acoustic propagation, we employ a successful path to Bermuda obtained for the March 15, 2004 iter22 state estimate obtained using 25-Hz frequency. The 2009 World Ocean Atlas (WOA09) (Locarnini et al., 2009; Antonov et al., 2009) and iter22 sound speed sections were extracted along this path. The acoustic propagation along these sections was computed using the parabolic equation method (PE) (Collins, 1993; Jensen et al., 1994; McDonald et al., 1994) to obtain detailed predictions of the depth-travel time arrival patterns (time fronts) at Bermuda (Fig. 14). An acoustic pulse centered on 22 Hz with 11 Hz bandwidth was first employed. With the sea floor modeled as both deep and flat, arrival patterns extend some 70 s, with the first 60 s of the pattern having greatly reduced intensity relative to the final mode-1 arrival. For these low frequencies and for the smooth ocean realization of WOA09, arrivals of individual modes are evident in the arrival pattern, including a distinct mode-1 arrival arriving last. Arrivals of modes 2–3 are apparent in the arrival pattern by the locations of the nulls, corresponding to the zero crossings of the mode functions. With the more realistic ocean variability captured by the ECCO2 state estimates, the mode-1 arrival is less distinct.

Using 40 ± 30 Hz acoustic frequencies that reflect better the estimated frequency spectrum described in Section 3, the PE calculation showed that mode coupling became vigorous at these slightly higher frequencies. The dependence of acoustic coherence on frequency has been observed experimentally (Wage et al., 2005; Worcester and Spindel, 2005). Finally, the various topographic features along the path (Kerguelen, Crozet Islands) stripped away the deeper-traveling acoustic energy, leaving only the last 25 s of the arrival pattern. The slowest acoustic energy travels along the sound channel axis. The observed arrival coda resulted from ocean variability causing incoherence and mode coupling within the acoustic signals, together with topographic clipping of the early part of the time front. The mode-1 travel time in the PE calculation, indicated by the latest arriving acoustic energy, differed from the travel time computed by integrating the mode-1 group speed along this path by less than 1 s.

7.2. Arrival coda by superposition

The observed arrival coda resulted from the superposition of the signals arriving along several ray paths as they converged on Bermuda. The arrival coda can therefore be computed by summing the arrival patterns computed for each ray path. The calculation would be more accurate using a three dimensional acoustic propagation technique, but the computational requirements to do such calculations for broadband acoustic signals are overly formidable (but see Chiu et al., 1994). Combining the several two-dimensional (range and depth) calculations obtained for the ray paths is a reasonable and tractable approximation. The calculation was further approximated by computing acoustic predictions using paths obtained for only 25-Hz frequency. Technically, a different set of ray paths would be obtained for each frequency and mode number, but the paths obtained within each ray group were similar. The mode-1 travel times were independent of frequency. Paths derived using 25-Hz frequency were used to ensure that a reasonable number of paths were employed, while using a frequency near the center of the expected spectrum.

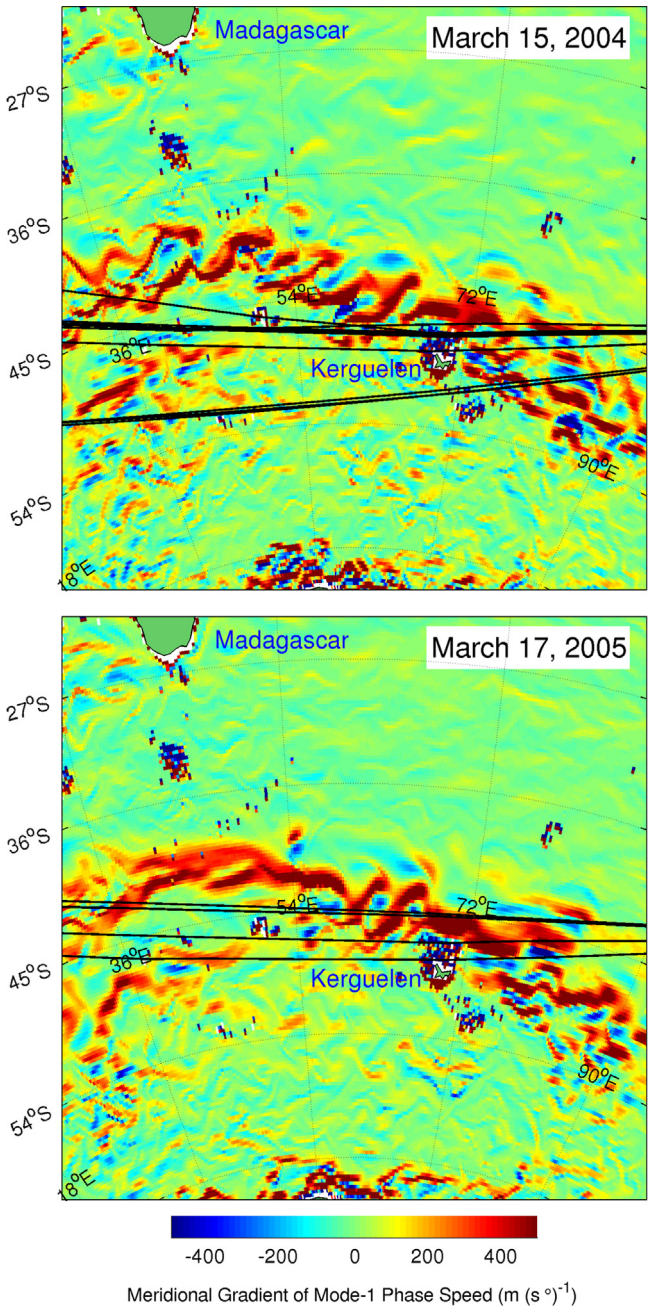

Fig. 13. Top: The meridional gradient of mode-1 phase speed derived from the iter22 ECCO2 solution for March 15, 2004, together with the ray paths to Bermuda obtained for this solution. Bottom: The same for the March 17, 2005 solution. With the iter22 solution, the nature of the sound speed gradients within the ACC has changes such that by 2005 more northerly ray paths are obtained. The change in ray paths is attributed to an unphysical artifact of the iter22 solution. Azimuthal equal area projection.

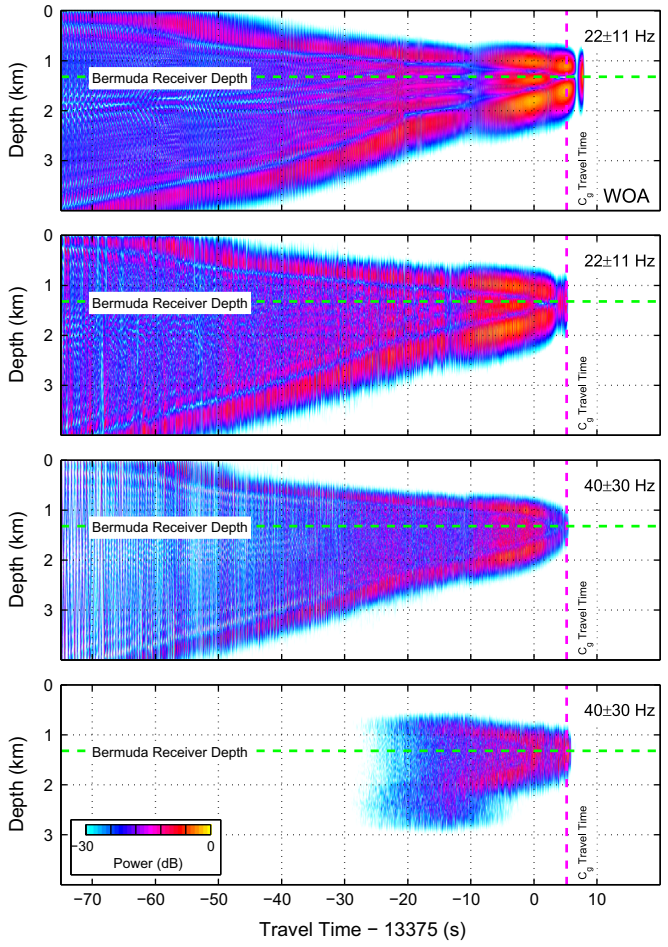

Fig. 14. The arrival pattern at Bermuda for a particular path between Perth and Bermuda on March 15, 2004 as computed by the parabolic equation method using: (a) The WOA09 sound speed section and a simulated acoustic pulse with 22-Hz center frequency and 11-Hz bandwidth. For this smooth ocean realization and low-frequency band, the arrival time front indicates clear low-mode arrivals (one can count the zero crossings within the time front) and a clear, distinguished mode-1 arrival. Absent topographic effects, the time front duration is about 70 s. (b) An ECCO2 state estimate realization for March 15, 2004 for the frequency band as in (a). The small-scale features of the ECCO2 estimate induce mode coupling such that a clear mode-1 arrival is no longer evident. The arrival time computed by integrating the ECCO2 mode-1 group speed along the path is indicated by the vertical dashed line; the mode-1 travel time in WOA09 lags by about 3 s. (c) Frequencies appropriate for the estimated frequency spectrum of the arrival pulses at Bermuda, about 40 ± 30 Hz. At these slightly higher frequencies mode coupling is more prevalent and individual mode characteristics of the time front are no longer evident. (d) As in (c), but including the sea-floor topography. The shoaling regions of the Kerguelen Plateau serve to strip away the faster, deeper-turning acoustic energy, leaving only the slowest-traveling part of the time front. This computed arrival pattern is similar to the measured arrival pulses.

The parabolic equation technique was used to compute the complex acoustic arrival pressure for each of the dozen or so rays arriving at Bermuda. These arrival patterns were summed and then processed to form a computed estimate for the arrival coda at Bermuda derived from the ECCO2 state estimates (Fig. 15). This superposition models what would occur in nature as acoustic signals on several paths converge and combine near Bermuda. The agreement between computed and measured arrival coda is excellent, with no change in travel time apparent between the 1960 measurements and the 2004 computations.

The PE computations took several days to complete. To test a faster approach, the calculation was repeated using geometric rays (Dushaw and Colosi, 1998) (rays computed in range and depth, not to be confused with the rays computed in latitude and longitude discussed heretofore), which gave results roughly equivalent to the PE (Fig. 15). The ray calculations took only a few minutes to complete, however. Amplitude was derived from the geometric ray time fronts by estimating ray density, converting the density to a log scale, and then ad hoc scaling the estimated intensity to be similar to the observations. Ray computations for several ECCO2 time averages were then obtained for comparison to the observations (Fig. 16).

For all of 2004, the arrival pattern consists of the double pulse arrival as observed, with little or no difference between computed and measured travel times (cf. Fig. 12). It is difficult to assess

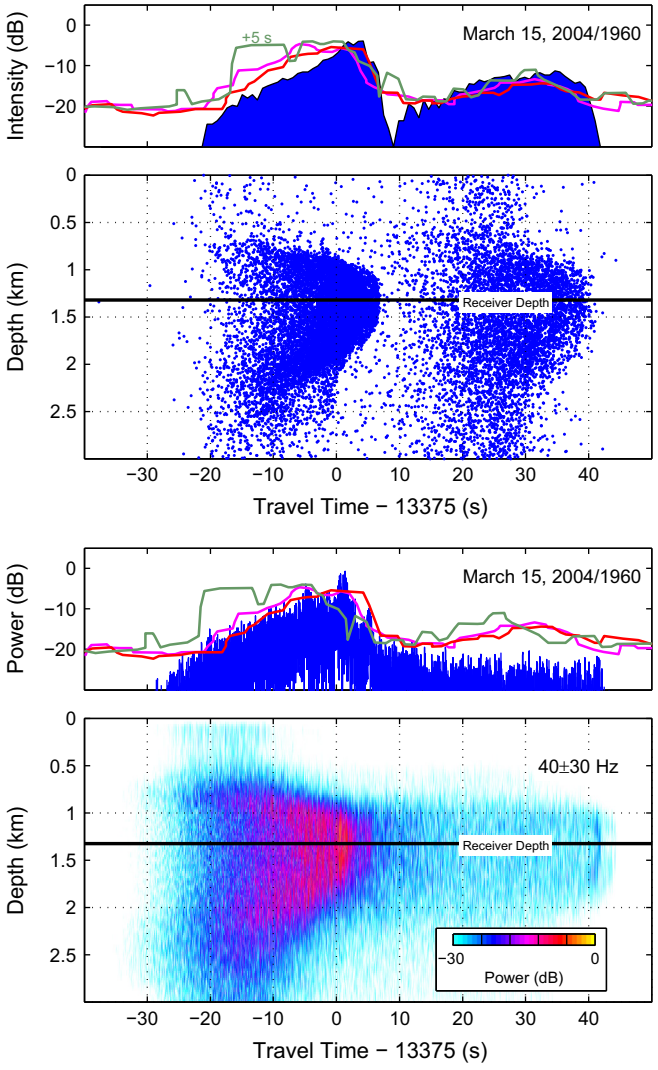

Fig. 15. Reconstruction of the arrival coda recorded at Bermuda using the ECCO2 state estimate for 15 March 2004 computed by summing the acoustic signals obtained on the several acoustic paths arriving at Bermuda. The bottom panels show the arrival pattern computed by summing the complex pressure signals derived using the parabolic equation, while the top panels show the equivalent arrival pattern computed by simple ray tracing. In both cases, the travel time and doublet pattern recorded in 1960, indicated by the three colored lines, is reproduced in detail, with no travel time change observed in 2004 compared to 1960. The last recorded arrival doublet, indicated by the green line, required a 5-s delay for it to align with the other two arrivals (Appendix); bottom panel uncorrected, top panel corrected. (For interpretation of the references to color in this figure caption, the reader is referred to the web version of this paper.)

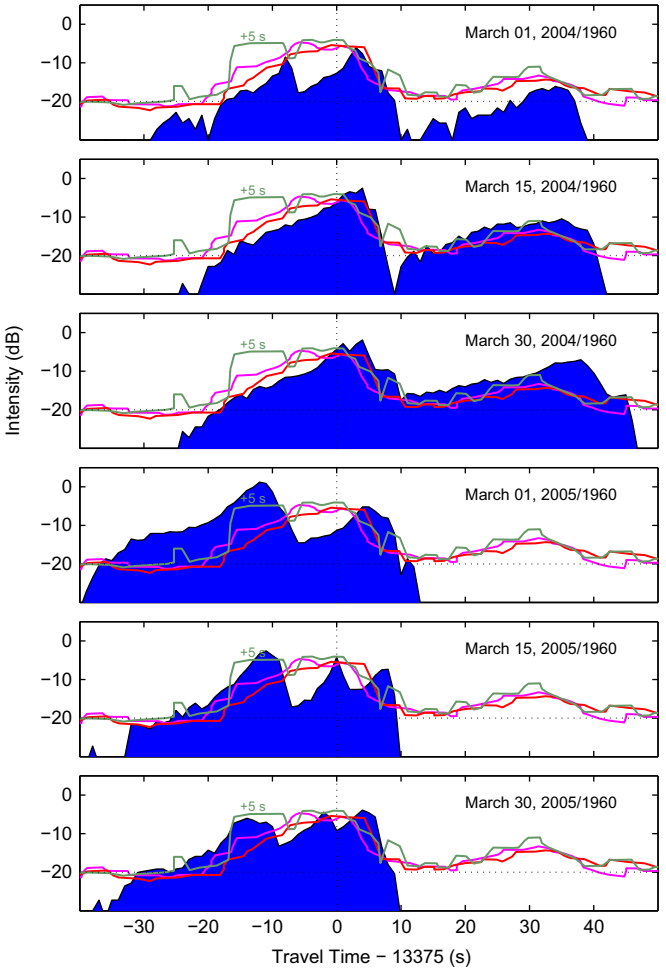

Fig. 16. Reconstructions of the arrival coda recorded at Bermuda computed by ray tracing for the six ECCO2 state estimates indicated in Fig. 10. During 2004, the arrival coda varied slightly, with little variation in travel time. During 2005, the second pulse arrival, associated with paths passing near Brazil, was not obtained, and a ca. 10-s decrease in travel time is observed. This travel time change was associated with a northward shift in paths as they cross the Indian Ocean, rather than with oceanic warming.

a precise difference in travel time between measured and predicted coda, but a simple correlation calculation suggests that the computed travel time is about 1 s less than the 1960 measurement, a difference much less than the estimated uncertainties, discussed next. As discussed earlier, the arrival patterns in the 2005 iter22 solution were not consistent with the observations, since the second ray group passing near Brazil was not obtained. Because of the different ray paths, the 2005 iter22 solution has a 10-s travel time discrepancy relative to 2004.

8. A measurement of climate change over 50 years

Although the comparisons above suggest there has been little change in travel time between 1960 and 2004, they have little meaning without a careful consideration of the uncertainties in the measurements and the calculations. The three dominant sources of uncertainty are the positioning of the three shots, a possible bias in the ECCO2 ocean state estimates, and the geophysical variability of the travel times associated with the movements of fronts, the mesoscale, or the meanders of the ray paths. The equation for sound speed is accurate to about 0.2 m s^{-1} (Dushaw et al., 1993; Worcester et al., 1999), which corresponds to about 1 s uncertainty for the antipodal travel time. Our best assessment of these and other uncertainties, expressed as standard errors, are summarized in Table 1. Some uncertainties, such as the ECCO2 model bias, may be eventually remedied, in which case the computed and measured travel time comparison may become more constrained.

The determination of the source position is discussed in detail in the Appendix. It is evident that the officers of *HMAS Diamantina* paid particular attention to obtaining an accurate position estimate for the shot locations. The position determined by the captain of *HMAS Diamantina* was constrained by triangulation from landmarks the evening before the shots, and a celestial observation at dawn 3 h after the shots. The uncertainty in position is not random, however, since the position has the additional constraint that the depth at the location of the charges was reported. The "true" position could have been up to 7 km

Table 1
Travel time standard error budget. Values of "Nil" are given for errors much less than 1 s. Source location and timing errors are discussed in the Appendix. The source location error acts only to reduce travel time, hence the distribution of uncertainty is asymmetrical about zero. Recall that under the formalism of standard errors, values of up to two standard deviations are likely, while values greater than two standard deviations are unlikely.

Source location (less than 7 km)	(−)3 s
Source timing	1 s
Receiver location	Nil
Receiver timing	Nil
ECCO2 state estimate bias	2 s
Computational error	Nil
Sound speed equation error (0.1 m/s)	1 s
Geophysical noise (1960)	3 s
Ocean currents	Nil
Total	−4.9/+3.8 s

westward, but not eastward, since the continental slope is shoaling rapidly in that direction. Errors in source position therefore act to close the range between the shot locations and Bermuda. With such a 7-km shift in source location, the computed travel times could be up to 5 s less than those obtained (Fig. A1). A standard error of 3 s, applicable only to reducing travel time, is therefore assumed for the contribution of position uncertainty to the travel time comparison. Fundamentally, the asymmetry in uncertainty stems from our reluctance to make our own determination of the position of *Diamantina* at the time of the shots. Absent strong contradictory evidence, we are loath to second guess the position estimated by the captain of *Diamantina* and his Navigation Officer. Nevertheless, we attempt a posteriori to estimate meaningful uncertainties, but this process is disconnected from that used to determine the original position.

Ocean model drifts and biases are challenging problems for ocean state estimation, especially in the context of long-range acoustics where small biases in vertical or horizontal gradients can have large consequences for acoustic propagation (Dushaw et al., 2013). Assessing the magnitude of bias is equally challenging. One possible estimate of bias, however flawed, is the 3-s difference in travel times obtained using WOA09 and the ECCO2 solution apparent in the top panels of Fig. 14. An equivalent prediction computed from the World Ocean Circulation Experiment (WOCE) global hydrographic climatology (Gouretski and Kolterman, 2004) was delayed by an additional 4 s relative to WOA09 (not shown). At least some of the difference between the travel times for smoothed climatology and the ECCO2 state estimates may be attributed to the "mesoscale bias," or the small decrease in travel time induced by the fluctuating sound speeds of mesoscale variability (Munk and Wunsch, 1985, 1987). Munk et al. (1988) estimated a travel time bias of −0.7 s for 20,0000 km propagation. The mean travel times for mode 1 at 15 Hz derived from the cube78 and iter22 state estimates differed by less than 2 s. Relative to 2004 Argo profiling float data, we estimated that cube78 and iter22 may have a travel time bias of −5 s and −2 s, respectively. While by 2004 Argo sampling had not yet saturated in the Southern Ocean, there was still substantial available sampling around the Crozets and between Kerguelen and Australia. Further, iter22 annual-average sound speeds were negligibly different from sound speeds of the OCean Comprehensible Atlas (OCCA) (Forget, 2010), which corresponds to the 2003–2006 time period. Sound speeds of these estimates, averaged along the sound channel axis over the antipodal path, differed by only 0.2 m s^{-1}. From these considerations, as well as 1-s differences between observations and model predictions in the Pacific at 5-Mm range (Dushaw et al., 2013), we estimate the climatological bias of the ECCO2 state estimates could introduce a computed travel time uncertainty of up to 4 s. A standard error of 2 s is therefore assumed for the contribution of state estimate bias uncertainty to the travel time comparison.

The mode-1 travel time for paths arriving at Bermuda had 2.6 s RMS variability in the 15-year cube78 state estimate, while the 12-month iter22 state estimate (excluding 2005 because of the previously discussed problem) had 1.8 s RMS variability. These variabilities are fractions of the nominal 9-second signal expected from a half century of ocean warming. Another source of uncertainty arises from the decadal oceanic variability that is frequently observed. The magnitude of uncertainty from decadal-scale variability, antipodally averaged, is unknown, although the 15-y cube78 time series suggested remarkable travel time stability. To the extent that an annual-mean travel time can be computed for the present-day state, these uncertainties pertain only to the single 1960 travel time measurement. A standard error of 3 s is therefore assumed for the contribution of geophysical variability to the travel time comparison.

While it is possible for ocean currents to influence the acoustic propagation, this influence is insignificant compared to that arising from temperature. The strongest currents occur within the ACC with speeds O(1 m/s). Even these large currents are dwarfed by sound speed variabilities arising from temperature variabilities, where a 1 °C change in temperature corresponds to 4.5 m s^{-1} change in sound speed. Further, for currents to have much effect on acoustic mode propagation they must have considerable vertical and horizontal extent; a near-surface jet of current would have little effect. The acoustic pulses did not spend much time within the ACC, hence it had minimal effect on the travel times. The contribution of currents to travel time was quantified by computing average currents of the upper ocean along the antipodal path using the current fields of the ECCO2 state estimates. The time-mean average current was about 0.4 mm s^{-1}, while the RMS current was about 2 mm s^{-1}. Such currents have a negligible effect (0.02 s) on antipodal travel times.

Combining all uncertainties by making the crude approximation that the statistics are Gaussian, the net standard errors for the travel time comparison were −4.9/+3.8 s. If a −9.4-s signal corresponds to +5 m °C yr^{-1} warming, the probabilities for average warming rate between 1960 and 2004 are: −4.1 to −2.0 m °C yr^{-1} (12%), −2.0 to 0.0 m °C yr^{-1} (29%), 0.0 to 2.7 m °C yr^{-1} (39%), and 2.7 to 5.2 m °C yr^{-1} (15%), leaving 5% chance for values outside these ranges. Note that these numbers suggest a 41% chance of cooling by a few m °C yr^{-1}, against a 54% chance of warming. Alternatively, this comparison indicates that warming rate has been less than 4.6 m °C yr^{-1} at 95% confidence. It is to be emphasized that this measurement is averaged along the sound channel axis (Fig. 17).

9. The Longuet-Higgins explanation for the doublet arrival

Longuet-Higgins (1990) proposed an elegant explanation for the doublet arrivals shown in Fig. 1. He suggested that the double arrival was a product of the ray path caustics that occur for antipodal rays traveling over an oblate spheroid. Because of the oblateness, rays of various azimuthal angles intersect to form a well-defined star-like caustic pattern (multiple rays at the same point) near the antipode. Although this explanation is intriguing, the calculation of the caustic pattern in practice showed that the area of the caustic was quite small and considerably displaced from the Bermuda receiver. The continents of South America and Africa form quite a narrow aperture for the antipodal rays, which greatly limits the area of the antipode caustic. This small area combined with the evident response of the rays to the ocean variability makes the Longuet-Higgins explanation unlikely.

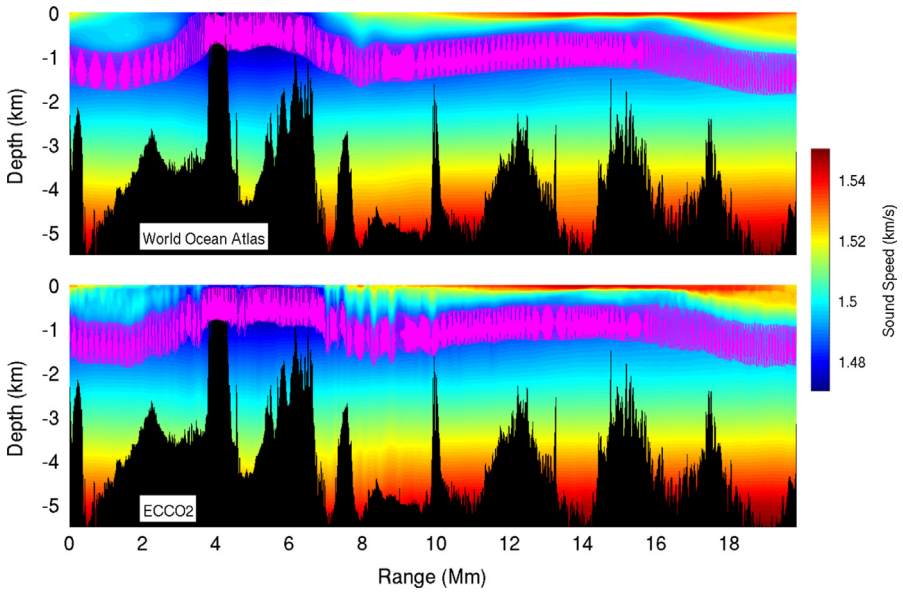

Fig. 17. Sound speed sections and a 1° acoustic ray along an acoustic path between Perth and Bermuda computed using the WOA09 (top) and the iter22 ECCO2 state estimate (bottom) for March 2004. The small-angle ray travels along the sound channel axis, approximately indicating the measurement kernel associated with the 1960 travel time measurement. The acoustic rays follow the undulations of sound speed associated with mesoscale variability, e.g., the Agulhas Rings at about 8 Mm range.

10. Discussion

There was no single path for the Perth-to-Bermuda acoustic propagation problem. Rather, multiple ray paths arose from the turbulent, filamental structure of the Antarctic circumpolar front and Southern Ocean. In addition, the rays interacted with the large sound speed perturbations of the Agulhas Rings. These refractive influences cause ray paths to meander back and forth and pass to the south of Bermuda by about 130 km. Without the influence of the sea floor, rays that arrive nearest to Bermuda pass near the Crozet Islands and well to the south of Cape Agulhas. In the 15-years of the ECCO2 cube78 state estimates there was no evidence of a change in ocean state that affects the basic nature of the acoustic propagation to Bermuda. This was not true for the iter22 state estimates, however, which obtained ray path solutions in 2005 with a more northerly route and about 10 s less travel time. We concluded that the 2005 ray paths resulted from model or estimation artifacts that caused unphysical changes in the horizontal sound speed gradients of the ACC (Fig. 13), however.

Although various analyses over the years looked for a single feature that would lend sufficient refraction to the rays to bend them toward Bermuda, no such single feature was found. Even the Agulhas Rings with sound speed perturbations of some 25 m/s do not on their own cause dramatic horizontal refraction of the rays. Rather, the meandering of the rays near Bermuda is an accumulation of many small contributions of refraction. The rare rays that managed to arrive at Bermuda without topographic interaction resulted from refraction during their propagation across the Southern Ocean that then gave them the right approach to a sequence of Agulhas Rings that then caused additional northward bending.

By including the influence of the sea floor, successful ray arrivals were obtained at Bermuda. Ray paths must scatter off of the seamounts of the Kerguelen Plateau and the Crozet Islands, and in doing so their signal levels are reduced some 20–30 dB relative to the direct arrivals. This reduction in signal explains some of the perplexity expressed by Hartegen and others in the historical documentation from the time of the experiment. The influence of the small-scale features of the ocean alone in refracting the ray paths closer to Bermuda is important in this regard. Without this influence, the acoustic rays would have had to scatter from topography into greater angles, with corresponding greater reduction in their intensity. The second, weaker arrival pulse arose from paths passing near the eastern tip of Brazil. The relative amplitudes computed for these two paths are in close agreement with the relative amplitudes of the measured pulses. These conclusions are essentially consistent with those of Heaney et al. (1991) and McDonald et al. (1994), with nuanced differences arising from the finer scales of ocean variability and topographic features available in present-day environmental data.

Arrival coda were computed using the iter22 ocean state estimates and compared to the coda measured in 1960. The computed and measured coda were in excellent agreement, with the computations obtaining double-pulsed coda with widths and travel times in agreement with the observations. No appreciable travel time change was apparent between 1960 and 2004. A consideration of the various uncertainties associated with the 1960 measurements and the 2004 calculations suggests that the ocean warming rate is less than 4.6 m °C yr^{-1} at the 95% confidence limit, with a 41% chance of cooling by a few m °C yr^{-1}. The three largest contributors to uncertainty were the 1960 source position (-5 to 0 s), the possible ECCO2 state estimate bias (up to ± 4 s), and the ocean variability (± 3 s). The antipodal travel times derived from the ECCO2 state estimates were remarkably stable. One may note that determination of a modest, rather than extraordinary, rate of temperature change was not a foregone conclusion.

The low-mode travel times are associated with the "measurement kernel" of their propagation, which is confined near the sound channel axis (Fig. 17). The Southern Ocean likely has the most influence on the travel times, since in that region the sound channel is near the surface where ocean temperature change is expected to be the largest. Over most of the antipodal path this axis lies at a depth of 1000–1500 m, so the lack of obvious evidence of warming is not inconsistent with the upper-ocean warming reported by Levitus et al. (2000, 2005, 2012) and others. Indeed the measurement is not inconsistent with warming of 20 m °C yr^{-1} within the Southern Ocean, and no warming along the sound channel axis elsewhere. To place the present result in the context of existing analyses, the Levitus et al. (2012) pentadal

fields for thermal anomaly were obtained (http://www.nodc.noaa.gov/OC5/3M_HEAT_CONTENT/). These global fields extend over the past six decades, and estimates for the anomaly extend from the surface to 2000 m. They are heavily smoothed in space and smoothed in time using a 5-year running mean. Along both the great circle and geodesic routes between Perth and Bermuda, the thermal anomalies were averaged over depths between 200 m above and below the sound channel axis (Fig. 18). This average approximates the measurement kernel associated with the acoustic propagation. The Levitus et al. (2012) estimates suggest that the sound channel axis has warmed by only 0.12 °C, corresponding to a travel time decrease of only about 5 s. While the difference between measured (1960) and computed (2004) travel times is nearly zero, the uncertainty of this result is within one standard error of the warming indicated by the Levitus et al. (2012) analyses (Fig. 18). The present comparison is thus not inconsistent with existing analyses, with only a modest suggestion of weaker warming along the sound channel axis.

It is natural to contemplate repeating the 1960 tests for an equivalent present-day measurement. A repeat test would give a full understanding of the frequency dependence and attenuation of the acoustic scattering from the Kerguelen and Crozets seamounts and provide a precise test combining concurrent state estimates and acoustic propagation. An exact repeat of the 1960 test would be required, including the deployment of 300-lb explosive shots, together with several additional receivers deployed in key regions, e.g., near the Crozets and Kerguelen islands, the southern tip of Africa, and the eastern tip of Brazil. Such an experiment would determine the exact nature of the acoustic signals at Bermuda, particularly its frequency dependence, and would be conducted during a time when considerable in situ data are available for an accurate state estimate by data assimilation and modeling. Such a test would not only give a present day measurement, it would confirm our understanding of the properties of antipodal acoustic propagation.

In any case, it is clear that it is possible to monitor the antipodally averaged temperature of the ocean, averaged along the sound channel axis, using acoustic techniques. The travel time uncertainty of new measurements conducted with modern technology would be just a fraction of a second, with weekly or even daily temporal resolution. Because the 1960 acoustic propagation interacted with rough topography in traveling to Bermuda, the design of a present-day monitoring configuration intended to build on the 1960 data is not so obvious. Without an initial exact replication of the 1960 test, any difference between 1960 and present-day travel times may have an ambiguous interpretation. Any observing system would be optimally designed to employ controlled low-frequency acoustic sources and acoustic paths that avoided topographic interaction, hence inherently different from the 1960 test. The advantage of antipodal acoustic thermometry for ocean observing may be questionable, inasmuch as such paths cross several climatological regimes of the ocean. We have seen how the acoustic approach presents tangible tests for ocean modeling and state estimation, however, and any such system would allow simultaneous acoustic measurements to be taken by any number of inexpensive receivers throughout the Southern Ocean.

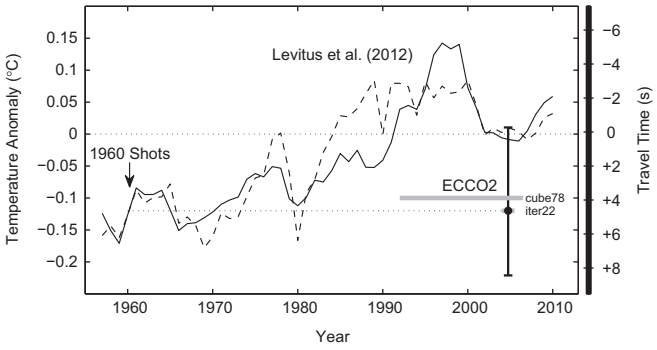

Fig. 18. Time series of temperature anomaly over five decades computed by averaging the Levitus et al. (2012) estimates near the sound channel axis over antipodal acoustic paths (great circle/dashed, geodesic/solid). Formally from these time series, the expected travel time decrease from 1960 to 2004 is only about 5 s, but the uncertainties are large. The intervals of the 15-year cube78 and 16-month iter22 ECCO2 solutions are indicated by the heavy gray lines, aligned to the temperature anomaly value for 1960. Travel times computed from the state estimates were little changed from the 1960 measurements, but the uncertainties associated with the comparisons (−4.9/+3.8 s) are comparable to the warming signal expected from Levitus et al. (2012).

Acknowledgments

This project was supported by National Science Foundation Grant OCE-0850357 and Office of Naval Research Grants N00014-09-1-0446, N00014-12-1-0183. D.M. performed this work at the Jet Propulsion Laboratory, California Institute of Technology, under contract with the National Aeronautics and Space Administration (NASA) Modeling Analysis and Prediction (MAP) Program. Thanks are due to Lieutenant Commander Ian Jempson RAN (Navigating Officer, ret.) of the Queensland Maritime Museum for providing essential assistance in the interpretation of the *HMAS Diamantina* Ship's Log and other information. We would like to thank the staffs of the National Archives of Australia and the Australian War Memorial for their helpful efficiency in locating and making available material related to *HMAS Diamantina* and the 1960 experiment.

Appendix A. The narrative of the *HMAS Diamantina* in March 1960

Many of the details of the Perth–Bermuda transmission experiment are unavailable or have been lost in the intervening half-century since the experiment was conducted. Insofar as we are using these data as a measure of ocean temperature in 1960, it is important to establish the accuracy of the timing and positioning of the acoustic sources and receivers.

Several primary and secondary references are available which give details of various aspects of the measurement. Two primary sources are Bryan et al. (1963), which give the experimental procedures for the acoustic shots by the *RV Vema* leading up to the shots by *Her Majesty's Australian Ship* (*HMAS*) *Diamantina*, and Shockley et al. (1982), which give the first report of the data and some of the details of the experiment. These references do not give a complete description of the experiment, however. A secondary source is the book on the history of *Diamantina* by Nunan (2005), based to a large extent on the ship's monthly proceedings. In the initial 1960 news report of the antipodal experiment (AGU, 1960), John Ewing suggests one motivation was to test the ability to monitor for clandestine underwater atomic blasts.

Historical research for the purposes of this project has turned up several additional documents. The most useful of these is the "Report of Proceedings" by the captains of the *Diamantina* for the month of March 1960 (HMAS Diamantina, 1960a). Appended to this report is an exchange of letters concerning the antipodal experiment between the captain of the *Diamantina*, Lieutenant Commander G. McC. Jude, RAN, and the associate director of the Bermuda SOFAR Station, Carl Hartdegen. The Ship's Log for *Diamantina* for March 1960 is also available (HMAS Diamantina, 1960b), which gives the ship's course and weather conditions

during the deployment of the shots. While somewhat cryptic and terse, the Ship's Log is specific about the actions and course of the ship; it demands careful interpretation. Finally, in 1960 *Diamantina* was a scientific ship on a hydrographic expedition, and the cruise report (CSIRO, 1962) puts the antipodal test shots in the context of the scientific activities of the *Diamantina* at the time.

Drawing from these references, this Appendix describes how *Diamantina* came to deploy the acoustic shots and the conditions of their deployment. The dominant experimental uncertainty is that of the positioning of the shots with about 7 km uncertainty. The uncertainty in position, resulting from a reliance on dead reckoning, is not random, however, with evidence that the true shot locations were slightly further west.

A.1. RV Vema in Winter 1959–1960

As reported by Bryan et al. (1963), during the winter 1959–1960 *Vema* (Cruise 16) conducted a transect across the tropical and southern Atlantic Oceans deploying a large number of 3- and 48-lb TNT charges at regular intervals. Professor of geophysics John Nafe of Lamont-Doherty Earth Observatory served as chief scientist. The acoustic signals from these shots were recorded by receiving arrays located near Fernando de Noronha and Ascension Islands. The need for careful positioning by celestial fix and time keeping for the shots was noted. At the end of this transect, *Vema* entered the Indian Ocean on a course with an abrupt left turn in order to test the shadowing effects of the African continent on the acoustic propagation to the receivers in the South Atlantic. Bryan et al. (1963) concluded "the continental land masses completely block the signal, and any bending of the ray paths around such land masses is less than about 3°." However, the analysis of Bryan et al. (1963) assumed a spherical earth and great circle paths, hence the conclusions concerning the blocking by the African continent were not precisely correct.

The nature of *Vema*'s transect is consistent with the experimental procedures for such tests dating back to the late 1930s (Ewing and Worzel, 1948). The Ewing and Worzel (1948) paper suggests that acoustic signals from a 4-lb shot would be capable of propagating antipodal distances. It seems evident that the antipodal tests of 1960 were aimed at verifying this long-suspected notion.

Vema arrived at Fremantle, Australia on 22 February 1960 from Mauritius. On 1 March, *Vema* dropped six 200-lb TNT shots at 33° 36′S 113° 29′E (Fig. A1) just off the Australian continental shelf with the signals recorded at Bermuda 3 h 41 min later. The arriving signals at Bermuda were weak. As Hartdegen stated in his letter to the captain of the *Diamantina*, "when the Vema shot, we had to rerun the magnetic tape several times and look for it [the signal] in the mud." The recorded signals from this set of tests are no longer available. The travel times for these shots vary by up to a minute (Shockley et al., 1982), most likely because of the weak signals. Based on the long history of the idea of antipodal propagation, the care with which the location of the shots was chosen, and the description of the experiment in the Shockley et al. (1982) paper, we infer that the location of the *Vema* shots was carefully chosen to give a clear antipodal path to Bermuda. Great circle, rather than geodesic, routes on the sphere were used for this purpose, however.

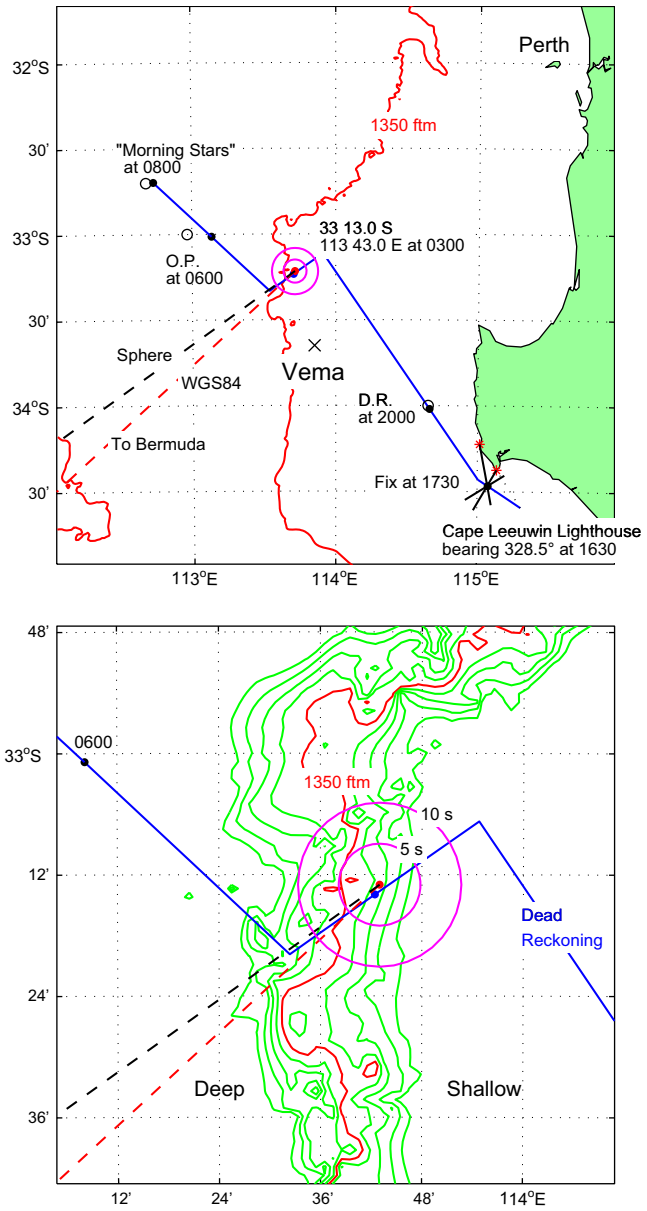

Fig. A1. Upper panel: The course of *HMAS Diamantina* on March 21–22, 1960, as reconstructed by dead reckoning from the Ship's Log. Positions noted in the Ship's Log are shown as the open circles. Accurate positions were determined by triangulation at 1730 and 1850, and the ship proceeded by dead reckoning (black dots) to the predetermined deployment location. The red dot denotes the captain's position for the shots. A celestial fix was obtained prior to dawn 3 h after the shots. The red line indicates the 1350 ftm contour, the reported depth at the shot location. The magenta circles indicate 7.5- and 15-km distance errors corresponding to 5- and 10-s travel time errors. The dashed black/red lines indicate the great circle/WGS84 routes to Bermuda. The "X" denoted "Vema" marks the location of the shots deployed on March 1 by RV Vema. Lower panel: The shot location, giving depth contours at 125-m (68-ftm) intervals. The depth at the reported location of the shots is shallower than 1350 ftm, suggesting that the true location of the shots was slightly further to the west. (For interpretation of the references to color in this figure caption, the reader is referred to the web version of this paper.)

A.2. HMAS Diamantina

HMAS Diamantina was a River Class frigate (named after rivers) built toward the end of World War II. These frigates were generally employed by the allies for convoy work during the war. *Diamantina* had seen minor action during World War II, particularly around Bougainville, but in 1959 she had been recommissioned as an oceanographic survey ship. In 1960, *Diamantina* was on her second scientific cruise (CSIRO, 1962). These cruises were staffed by Commonwealth Scientific and Research Organization (CSIRO) scientists and consisted of hydrographic, bathymetry, and biological surveys. At several times during this second cruise, *Diamantina* coordinated with *Vema* for seismic surveys along the Australian continental shelf, where one ship hove to in order to act as a receiving station, while the other ship dropped 1/2- to 300-lb

explosive charges. Relations between the two ships were described as excellent, and, indeed, *Diamantina* and *Vema* conducted similar joint seismic surveys several more times during the 1960s.

On March 2, *Vema* rendezvoused with *Diamantina* to begin the first instance of coordinated seismic profile work. *Diamantina* had left Fremantle the previous day. On March 13, *Vema* again met up with *Diamantina* on the northwestern end of Kangaroo Island, South Australia to return to *Vema* the stores and equipment used for the seismic work. At this time Professor Nafe made arrangements for *Diamantina* to fire the depth charges at a predetermined position on her return passage to Fremantle.

The exact rationale for these additional tests is unclear. Shockley et al. (1982) state, "Since the VEMA signals were rather weak, the participating scientists requested a repeat of the experiments with larger shots," but this does not seem correct inasmuch as a 300-lb shot offers only 1 dB greater signal than a 200-lb shot. The peak pressure from an explosive shot varies as the cube root of the yield, as was well known at the time (see, for example, Weston, 1960). In his letter to the captain of the *Diamantina*, Hartdegen states the opinion that the signals from the 300-lb shots "found a much better [topographic] hole," together with concerns about the reduction of the sound signal levels from shots detonating off the sound channel axis. We infer that the scientists involved were surprised by the weakness of the signals recorded at Bermuda from the 200-lb shots, and they assumed the signals had been blocked by some undersea topographic feature.

A.3. Off Perth, Australia at 3 am on March 22, 1960 (local)

At 1750 March 21 (local) *Diamantina* rounded Cape Leeuwin and steered a course of 325° to arrive at the predetermined site of the shots. At 2100 March 21 (local) the ship's speed was 10 kt. At 0200 March 22 (local), the ship changed course to 235° with speed 13 kt. The ship arrived on station a little before 3 am March 22 (local) and reduced speed to 4 kt. The Ship's Log notes: "0255 Commenced dropping 3 depth charges at 5 min intervals for seismic recording in Bermuda." These charges were deployed on course 235°, speed 4 kt. The different locations of the three shots, which span 0.67 nm, affect travel time to Bermuda by less than a second, since sound travels one nautical mile in about 1.2 s. In the Monthly Proceedings and in a letter to Hartdegen dated March 30, the captain noted that "the centre charge was dropped in position 33°13′0S, 113°43′0E." The weather at the time was clear skies and 30-mile visibility. The wind was force 5 (ca. 20 kt), 145°. The sea was 3′, and the swell was 6′, 190°. The Ship's Log notes: "0320 Completed firing run" and at that time the ship's speed increased to 13 kt with unchanged heading. At 0400, *Diamantina* changed course to 313° toward the location of its next hydrographic station, a revisit to the first hydrographic station of the cruise.

This sequence of actions by the *Diamantina* suggests this deployment had a simple, but effective strategy. The course and speed change at 0200 to 235°, 13 kt was likely meant to bring the *Diamantina* to the predetermined location for the shots, just off the continental shelf, by 0300 on an optimal heading. The course is, within a degree, along the great circle route to Bermuda; the course has no apparent relation to the weather or sea state. The advantage in the deployment of the shots along this heading is that the three sound signals would follow the identical antipodal path. In the nature of antipodal geodesics, deployment on a heading perpendicular to the great circle route would result in three different paths. That the ship continued on the same course for another 40 min at 13 kt after completing the firing run suggests that depth soundings were obtained to verify the acoustic signals that had cleared the continental shelf. In his letter to the *Diamantina* dated March 22, Hartdegen begins, "All of us here have a great deal of admiration for the way you were able to make sense and organize so nicely our recent shooting operation."

The captain's statements suggest an accurate location for the shots, but an accurate position measurement at that time is not recorded in the Ship's Log. Rather, the Log indicates that at 1730 and 1850 the previous evening, accurate positions for the ship were obtained by triangulation using landmarks on Cape Leeuwin (Fig. A1). In addition, a celestial fix (Morning Stars) was obtained prior to dawn about 3 h after the shot deployments. The Ship's Log records speed and direction, from which positions can be computed by dead reckoning. The ship's heading was recorded by Mk14 gyro compass, while speed through the water was recorded by electromagnetic log. Both these reliable pieces of equipment would have been calibrated when the ship was recommissioned in 1959 (Lt. Cmdr. I. Jempson RAN (ret.), personal communication, 2012). The course of the *Diamantina* is reconstructed in Fig. A1 by dead reckoning from the 1730 position. This reconstruction was also obtained independently by Lt. Cmdr. I. Jempson RAN, a retired Navigation Officer (personal communication, 2012). A 3% adjustment to the ship's speed has been applied, which brings the dead-reckoning positions into close alignment with the 2000 position, the captain's shot position, and the 0800 position (Fig. A1). Without this correction, the shot position reported by the captain lies about 7 km to the northwest of the reconstructed position, and the official position for the ship at 0800 noted in the Log, based on the observation of "Morning Stars", also lies to the northwest of the dead-reckoning position (Fig. A1). The "Dead Reckoning" position noted in the Log at 2000 shows that *Diamantina* was aware of the need for a speed correction. Inasmuch as the reconstructed course obtains an 0800 position consistent with that given by the Ship's Log, the speed correction is evidently consistent with the celestial fix obtained just before dawn. The shot position is constrained by both the triangulation positions obtained the prior evening and the celestial fix obtained 3 h after the shots. The 0800 position was also that of a hydrographic station, number D113/60 (CSIRO, 1962). Positioning discrepancies of O(200 m) may be accounted for by the (unknown) geodetic datum employed by *Diamantina* in 1960, rather than the WGS'84 datum employed here.

At 0600 a position is noted in the Log as "O.P." (Observed Position) (Fig. A1). Lt. Cmdr. I. Jempson (personal communication 2012) noted: "On 22 Mar Diamantina experienced sunrise at 0635 [noted in the Log]. Therefore, morning civil twilight [MCT] would have been at about 0625 and the horizon is usually clear enough to take accurate sights for about 10 minutes before MCT. By MCT all stars will be invisible. In summary they had from about 0615 to 0625 to take sextant sights." The "O.P" position is inconsistent with the 0800 position and the captain's shot location, however. Indeed, if the ship had been at the "O.P." position at 0600, it would have required a course and speed change to get to the 0800 position, but no such changes are noted in the Log. The "O.P." position therefore appears to be a Log entry to note the time and approximate location at which the celestial observations were obtained. The Log notes the weather at this time as blue skies and 10–30 mile visibility. The captain of *HMAS Diamantina* and his officers would have had all this information and more at hand as they made their determination of the ship's position.

The reported depth of the sea floor at the location of the shots was 2469 m (1350 ftm). This depth was compared to the sea-floor topography in the region (Fig. A1). The sea-floor topography employed for this purpose was Smith–Sandwell/SRTM30_PLUS V.8.0 with 30-s resolution (Smith and Sandwell, 1997; Becker et al., 2009). The stated depth at the time of the shots is 140 m (77 ftm) deeper than that calculated from the topographic data for the stated location of the shots. One should note that the accuracy of the reported depth, and its coincidence with the time of the shots, is unknown. It is certain that *Diamantina* employed an echo

sounder to determine depth (attempts to locate the original echo sounder chart, while ambitious, have not been successful). The Smith–Sandwell/SRTM30 data in the area was compared to 50-m resolution data obtained from multibeam echosounders provided by Geoscience Australia. (http://www.ga.gov.au/marine/bathymetry/50m-multibeam-dataset-of-Australia-2012.html Data available as of August 2012.) While this sampling did not cover the precise shot location, considerable sampling within 5–10 km of the shot location was available. Along the 1350 ftm contour, the Smith–Sandwell/SRTM30 data agreed with the multibeam data, except for short-scale (ca. 5 km) deviations in depth of about 50 m (27 ftm); no bias between the two data sets was evident. The topographic evidence and the reported depth at the time of the shots suggests that the true location was slightly further westward in deeper water. The true location is not likely to be eastward, since the sea floor is rapidly shoaling with the continental slope in that direction. The shots would certainly not have been deployed in shallower water, since such a deployment would have adversely affected the shot signals.

"Exact times" of detonation were measured with a "chronometer deck watch under difficult conditions," and these times were immediately relayed to the Bermuda SOFAR station by Canberra Radio. The chronometer was likely the ship's navigation clock, with a nominal accuracy of about 1 s. The times of detonation were 19 h 04 min 11 s, 19 h 09 min 43 s, and 19 h 15 min 07 s on March 21 (GMT) (the third time was initially reported as 19 h 14 min 07 s, but later corrected by *Diamantina*'s captain). We suggest that about 1 s should be subtracted from these times to account for the distance from the detonation at around 800 ftm to the ship, but we have not done this.

As noted in Figs. 14 and 15, the recorded coda for third shot led the other two by 5 s. This difference was not oceanographic inasmuch as the two pulses of the coda are associated with different ray groups, but the entire coda appears to be offset. It is not possible for the difference to arise from errors in the source position, the receiver position, or detonation times. An explanation for the 5-s difference is not likely to be determined with certainty, but, as just noted, there was some initial confusion in the time reported for the third shot. The likely explanation is that the time for the third shot was erroneously reported late by 5 s, that is, the shot actually occurred at 19 h 15 min 02 s.

Each depth charge consisted of 300-lb Amatol, three pressure detonators provided by *Vema*, two primers, one 1/2-lb charge TNT, and 1 lb of plastic explosive. Amatol, a mixture of TNT and ammonium nitrate, has an explosive yield roughly equivalent to TNT (Shockley et al., 1982; Navy Department, 1947). The detonators were set to explode at 800 ftm, but according to Shockley et al. (1982), based on Hartdegen's unpublished notes, "All shots used rather poor pressure detonators, which fired between 732 and 1800 m." *Diamantina* did not have a means of recording the explosive signals and their reflection from the sea floor, hence the precise depths of detonation could not be determined. Approximate detonation depths may be estimated from the available information, however. If the charges are assumed to have been dropped at 0255:00, 0300:30, and 0306:00 (cf. shot spacings in Fig. 1), then the charges descended for about 9 min 11 s, 9 min 13 s, and 9 min 7 s before detonating. 300-lb depth charges descend at about 3 m s^{-1} (Graves, 2003), so, based on these assumed descent times, the detonation depths of the shots differed by about 18 m, centering on about 1650 m (902 ftm).

A.4. The Bermuda SOFAR Station

By 1960, the Bermuda SOFAR Station had been operating for over a decade (AIP, 1996). This facility had been installed in 1949 for research and operational purposes by Gordon Hamilton for the U.S. Navy. Its original highly classified purpose, according to Hamilton, was to detect undersea atomic tests near Novala Zemla, north of Russia. The positions of the hydrophones, which were cabled to shore, were well known. The Bermuda receiver (Juliet) was located at 32°.17 N, 295°.42E, at a depth of 1323 m. Time keeping at this station was kept using WWV radio (Shockley et al., 1982), broadcast by the U.S. National Institute of Standards and Technology, with an accuracy of less than 10 ms. Munk et al. (1988) state that "the Bermuda receiver (an electrodynamic receiver) peaked at 150 Hz with a −6 dB/octave drop off to both sides." While we were not able to locate an original reference for this description, we note that Hamilton was a reviewer of the Munk et al. (1988) paper (Hamilton, 1988).

References

AGU, 1960. Notes and personalia. Eos Trans. AGU 41, 670.

AIP, 1996. Interview of Dr. Gordon Hamilton by Ron Doel on March 15, 1996. Niels Bohr Library & Archives, American Institute of Physics, College Park, MD, USA. ⟨http://www.aip.org/history/ohilist/6943_1.html⟩.

Aki, K., Richards, P., 1980. Quantitative Seismology, Theory and Methods, 2 vols. Freeman, San Francisco.

Antonov, J.I., Seidov, D., Boyer, T.P., Locarnini, R.A., Mishonov, A.V., Garcia, H.E., Baranova, O.K., Zweng, M.M., Johnson, D.R., 2009. World Ocean Atlas 2009. Salinity, vol. 2. NOAA Atlas NESDIS 68. U.S. Government Printing Office, Washington, DC, 184 pp.

Becker, J.J., Sandwell, D.T., Smith, W.H.F., Braud, J., Binder, B., Depner, J., Fabre, D., Factor, J., Ingalls, S., Kim, S.H., Ladner, R., Marks, K., Nelson, S., Pharaoh, A., Trimmer, R., Rosenberg, J.V., Wallace, G., Weatherall, P., 2009. Global bathymetry and elevation data at 30 arc seconds resolution: SRTM30_PLUS. Mar. Geod. 32, 355–371.

Bryan, G.M., Truchan, M., Ewing, J.I., 1963. Long-range SOFAR studies in the South Atlantic Ocean. J. Acoust. Soc. Am. 35, 273–278.

Chiu, C.S., Semtner, A.J., Ort, C.M., Miller, J.H., Ehret, L.L., 1994. A ray variability analysis of sound transmission from Heard Island to California. J. Acoust. Soc. Am. 96, 2380–2394.

Collins, M.D., 1993. A split-step Padé solution for the parabolic equation method. J. Acoust. Soc. Am. 93, 1736–1742.

CSIRO, 1962. Oceanographical Observations in the Indian Ocean in 1960. H.M.A.S. Diamantina cruise Dm1/60. Oceanographical Cruise Report No. 2. Technical Report. Division of Fisheries and Oceanography, CSIRO, Australia, 153 pp. ⟨http://www.marine.csiro.au/marq/edd_search.Browse_Citation?txtSession=5111⟩.

Del Grosso, V.A., 1974. New equation for speed of sound in natural waters (with comparisons to other equations). J. Acoust. Soc. Am. 56, 1084–1091, http://dx.doi.org/10.1121/1.1903388.

Divins, D.L., 2003. Total Sediment Thickness of the Worlds Oceans and Marginal Seas. NOAA National Geophysical Data Center, Boulder, CO

Dushaw, B.D., 2008. Another look at the 1960 Perth to Bermuda long-range acoustic propagation experiment. Geophys. Res. Lett. 35, L08601, http://dx.doi.org/10.1029/2008GL033415.

Dushaw, B.D., Colosi, J.A., 1998. Ray Tracing for Ocean Acoustic Tomography. Applied Physics Laboratory, University of Washington APL-UW TM 3-98.

Dushaw, B.D., Worcester, P.F., Dzieciuch, M.A., Menemenlis, D., 2013. On the time-mean state of ocean models and the properties of long-range acoustic propagation. J. Geophys. Res. 118, 4346–4362, http://dx.doi.org/10.1002/jgrc.20325.

Dushaw, B.D., Worcester, P.F., Cornuelle, B.D., Howe, B.M., 1993. On equations for the speed of sound in seawater. J. Acoust. Soc. Am. 93, 255–275.

Dushaw, B.D., Worcester, P.F., Munk, W.H., Spindel, R.C., Mercer, J.A., Howe, B.M., Metzger, K., Birdsall, T.G., Andrew, R.K., Dzieciuch, M.A., Cornuelle, B.D., Menemenlis, D., 2009. A decade of acoustic thermometry in the North Pacific Ocean. J. Geophys. Res. 114, C07021, http://dx.doi.org/10.1029/2008JC005124.

de Groot-Hedlin, C., Blackman, D., Jenkins, C., 2007. Hydroacoustic propagation through the Antarctic Convergence Zone: study of errors in yield and location estimates for explosive charge. In: 29th Monitoring Research Review: Ground-Based Nuclear Explosion Monitoring Technologies. National Nuclear Security Administration, Washington, DC, pp. 697–706.

de Groot-Hedlin, C.D., 2005. Estimation of the rupture length and velocity of the Great Sumatra earthquake of December 26, 2004 using hydroacoustic signals. Geophys. Res. Lett. 32, 4749–4765, http://dx.doi.org/10.1029/2005GL022695.

Ewing, M., Worzel, J.L., 1948. Long range sound transmission. In: Propagation of Sound in the Ocean. Memorials Geological Society of America, vol. 27. Geological Society of America, pp. 1–35.

Forget, G., 2010. Mapping ocean observations in a dynamical framework: a 2004–2006 ocean atlas. J. Phys. Oceanogr. 40, http://dx.doi.org/10.1175/2009JPO4043.1.

Gille, S.T., 2008. Decadal-scale temperature trends in the southern hemisphere ocean. J. Clim. 21, 4749–4765.

Gouretski, V.V., Kolterman, K.P., 2004. WOCE Global Hydrographic Climatology. Berichte des bundesamtes fur seeschifffahrt un hydrographie. Technical Report 35, 52 pp.

Graves, D.E., 2003. In Peril on the Sea: The Royal Canadian Navy and the Battle of the Atlantic. Robin Brass Studio, Inc.
Hamilton, E.L., 1980. Geoacoustic modeling of the sea floor. J. Acoust. Soc. Am. 68, 1313–1340.
Hamilton, E.L., 1987. Acoustic properties of sediments. In: Lara-Saenz, A., Ranz-Guerra, C., Carbo-Fite, C. (Eds.), Acoustics and the Ocean Bottom. C.S.I.C., Madrid, Spain, pp. 3–58
Hamilton, G., 1988. G.R. Hamilton to Dr. Eli Joel Katz, 1988. Scripps Institution of Oceanography Archives, University of California, San Diego Libraries "190. Australia-Bermuda Sound Transmission Experiment (1960) Revisited." Walter Munk Papers, MC17, 87-35, Box 26, April 12.
Heaney, K.D., Kuperman, W.A., McDonald, B.E., 1991. Perth–Bermuda sound propagation (1960): adiabatic mode interpretation. J. Acoust. Soc. Am. 90, 2586–2594.
HMAS Diamantina, 1960a. Reports of Proceedings for HMAS Diamantina, March 1960. Series AWM78, 99/3. National Archives of Australia/Australian War Memorial, 17 pp. ⟨http://recordsearch.naa.gov.au/SearchNRetrieve/Interface/DetailsReports/ItemDetail.aspx?Barcode=656251⟩.
HMAS Diamantina, 1960b. Ship's Log Book HMAS Diamantina, March 1960. Series SP707/1. National Archives of Australia/Sydney, 66 pp. ⟨http://recordsearch.naa.gov.au/SearchNRetrieve/Interface/DetailsReports/ItemDetail.aspx?Barcode=7530827⟩.
Jensen, F.B., Kuperman, W.A., Porter, M.B., Schmidt, H., 1994. Computational Ocean Acoustics. American Institute of Physics, Woodbury, NY
Levitus, S., Antonov, J., Boyer, T., 2005. Warming of the world ocean 1955–2003. Geophys. Res. Lett. 32, L02604, http://dx.doi.org/10.1029/2004GL021592.
Levitus, S., Antonov, J.I., Boyer, T.P., Baranova, O.K., Garcia, H.E., Locarnini, R.A., Mishonov, A.V., Reagan, J.R., Seidov, D., Yarosh, E.S., Zweng, M.M., 2012. World ocean heat content and thermosteric sea level change (0–2000 m) 1955–2010. Geophys. Res. Lett. 39, L10603. http:dx.doi/org.10.1029/2012GL051106.
Levitus, S., Antonov, J.I., Boyer, T.P., Stephens, C., 2000. Warming of the world ocean. Science 287, 2225–2229.
Locarnini, R.A., Mishonov, A.V., Antonov, J.I., Boyer, T.P., Garcia, H.E., Baranova, O.K., Zweng, M.M., Johnson, D.R., 2009. World ocean atlas 2009. Temperature, vol. 1. NOAA Atlas NESDIS 68. U.S. Government Printing Office, Washington, DC, 184 pp.
Longuet-Higgins, M., 1990. Ray paths and caustics on a slightly oblate ellipsoid. Proc. R. Soc. Lond. Ser. A 428, 283–290.
Lovett, J.R., 1980. Geographic variation of low-frequency sound absorption in the Atlantic, Indian, and Pacific Oceans. J. Acoust. Soc. Am. 67, 338–340.
Lyman, J.M., Good, S.A., Gouretski, V.V., Ishii, M., Johnson, G.C., Palmer, M.D., Smith, D.M., Willis, J., 2010. Robust warming of the global upper ocean. Nature 465, 334–337, http://dx.doi.org/10.1038/nature09043.
McDonald, B.E., Collins, M.D., Kuperman, W.A., Heaney, K.D., 1994. Comparison of data and model predictions for Heard Island acoustic transmissions. J. Acoust. Soc. Am. 96, 2357–2370.
Menemenlis, D., Campin, J., Heimbach, P., Hill, C., Lee, T., Nguyen, A., Schodlock, M., Zhang, H., 2008. ECCO2: high resolution global ocean and sea ice data synthesis. Mercator Ocean Q. Newsl. 31, 13–21.
Menemenlis, D., Fukumori, I., Lee, T., 2005a. Using Greens functions to calibrate an ocean general circulation model. Mon. Weather Rev. 133, 1224–1240.
Menemenlis, D., Hill, C., Adcroft, A., Campin, J., Cheng, B., Ciotti, B., Fukumori, I., Heimbach, P., Henze, C., Koehl, A., Lee, T., Stammer, D., Taft, J., Zhang, J., 2005b. NASA supercomputer improves prospects for ocean climate research. Eos Trans. AGU 86 89, 95–96.
Munk, W., Forbes, A.M.G., 1989. Global ocean warming: an acoustic measure?. J. Phys. Oceanogr. 19, 1765–1778.
Munk, W., Wunsch, C., 1985. Biases and caustics in long-range acoustic tomography. Deep-Sea Res. 32, 1317–1346.
Munk, W., Wunsch, C., 1987. Bias in acoustic travel time through an ocean with adiabatic range-dependence. Geophys. Astrophys. Fluid Dyn. 39, 1–24.
Munk, W., Zachariasen, F., 1991. Refraction of sound by islands and seamounts. J. Atmos. Ocean. Technol. 8, 554–574.
Munk, W.H., O'Reilly, W.C., Reid, J.L., 1988. Australia–Bermuda sound transmission experiment (1960) revisited. J. Phys. Oceanogr. 18, 1876–1898.
Munk, W.H., Spindel, R.C., Beggeroer, A., Birdsall, T.G., 1994. The Heard Island feasibility test. J. Acoust. Soc. Am. 96, 2330–2342.
Munk, W.H., Worcester, P.F., Wunsch, C., 1995. Ocean Acoustic Tomography. Cambridge University Press, Cambridge, England
Navy Department, 1947. U.S. Explosive Ordnance, OP 1664, vol. 1. Technical Report. Bureau of Ordnance, Washington, DC.
Nunan, P., 2005. HMAS Diamantina: Australia's Last River Class Frigate, 1945–1980. Slouch Hat Publications, McCrae, Vic., Australia
Porter, M.B., Reiss, E.L., 1985. A numerical method for bottom interacting ocean acoustic normal modes. J. Acoust. Soc. Am. 77, 1760–1767.
Press, W.H., Teukolsky, S.A., Vetterling, W.T., Flannery, B.P., 1992. Numerical Recipes in FORTRAN. Cambridge University Press, Cambridge, England
Prior, M.K., Meless, O., Bittner, P., Sugioka, H., 2011. Long-range detection and location of shallow underwater explosions using deep-sound-channel hydrophones. IEEE J. Ocean. Eng. 36, 703–715.
Shang, E.C., Wang, Y.Y., Georges, T.M., 1994. Dispersion and repopulation of Heard-Ascension modes. J. Acoust. Soc. Am. 96, 2371–2379.
Shockley, R.C., Northrop, J., Hansen, P.G., Hartdegen, C., 1982. SOFAR propagation paths from Australia to Bermuda: comparison of signal speed algorithms and experiments. J. Acoust. Soc. Am. 71, 51–60.
Smith, W.H.F., Sandwell, D.T., 1997. Global seafloor topography from satellite altimetry and ship depth soundings. Science 277, 1957–1962.
Talandier, J., Hyvernaud, O., Reymond, D., Okal, E.A., 2006. Acoustic signals generated by parked and drifting icebergs in the Southern Indian and Pacific Oceans. Geophys. J. Int. 165, 817–834, http://dx.doi.org/10.1111/j.1365-246X.2006.02911.x.
Urick, R.J., 1983. Principles of Underwater Sound. McGraw-Hill Book Company New York
Vincenty, T., 1975. Direct and inverse solutions of geodesics on the ellipsoid with applications of nested equations. Surv. Rev. 176, 88–93.
Wage, K.E., Dzieciuch, M.A., Worcester, P.F., Howe, B.M., Mercer, J.A., 2005. Mode coherence at megameter ranges in the North Pacific Ocean. J. Acoust. Soc. Am. 117, 1565–1581.
Weston, D.E., 1960. Underwater explosives as acoustic sources. Proc. Phys. Soc. Lond. 76, 233–249.
Worcester, P.F., Cornuelle, B.D., Dzieciuch, M.A., Munk, W.H., Howe, B.M., Mercer, J.A., Spindel, R.C., Colosi, J.A., Metzger, K., Birdsall, T.G., Baggeroer, A.B., 1999. A test of basin-scale acoustic thermometry using a large-aperture vertical array at 3250-km range in the eastern north pacific ocean. J. Acoust. Soc. Am. 105, 3185–3201.
Worcester, P.F., Spindel, R.C., 2005. North Pacific acoustic laboratory. J. Acoust. Soc. Am. 117, 1499–1510.
Wunsch, C., Heimbach, P., Ponte, R.M., Fukumori, I., 2009. The global general circulation of the ocean estimated by the ECCO-consortium. Oceanography 22, 88–103.